Measurement report: Enhanced photochemical formation of formic and isocyanic acids in urban region aloft: insights from tower-based online gradient measurements

Qing Yang[1], Xiao-Bing Li[1,*], Bin Yuan[1,*], Xiaoxiao Zhang[1], Yibo Huangfu[1], Lei Yang[1], Xianjun He[1], Jipeng Qi[1], Min Shao[1]

[1] College of Environment and Climate, Institute for Environmental and Climate Research, Guangdong-Hongkong-Macau Joint Laboratory of Collaborative Innovation for Environmental Quality, Jinan University

[*] Corresponding authors: Xiao-Bing Li (lixiaobing@jnu.edu.cn), Bin Yuan (byuan@jnu.edu.cn)

Abstract

Formic acid is the most abundant organic acid in the troposphere and has significant environmental and climatic impacts. Isocyanic acid poses severe threats to human health and could be formed through the degradation of formic acid. However, the lack of vertical observation information has strongly limited the understanding of their sources, particularly in urban regions with complex pollutant emissions. To address this issue, we assessed the impact of long tubes on the measurement uncertainties of formic and isocyanic acids and found that the tubing impact was negligible. Then, we conducted continuous (27 days) vertical gradient measurements (five heights between 5-320 m) of formic and isocyanic acids using long tubes based on a tall tower in Beijing, China, in the summer of 2021. Results show that the respective mean mixing ratios of formic and isocyanic acids were 1.3±1.3 ppbv and 0.28±0.16 ppbv at 5 m and were 2.1±1.9 ppbv and 0.43±0.21 ppbv at 320 m during the campaign. The mixing ratios of formic and isocyanic acids were substantially enhanced in daytime and correlated with the diurnal change of ozone. Upon sunrise, the mixing ratios of formic and isocyanic acids at different heights simultaneously increased even in the residual layer. In addition, positive vertical gradients were observed for formic and isocyanic acids throughout the day. The positive vertical gradients of formic and isocyanic acids in daytime imply the enhancement of their secondary formation in urban regions aloft, predominantly due to the enhancements of oxygenated volatile organic compounds. Furthermore, the afternoon peaks and positive vertical gradients of formic and isocyanic acids in nighttime also indicate their minor contributions from primary emissions from ground-level sources. The formation pathway of isocyanic acid through HCOOH-CH_3NO-HNCO was enhanced with height but only accounted for a tiny fraction of its ambient abundance. The abundance and source contributions of formic and isocyanic acids in the atmospheric boundary layer may be highly underestimated when being derived from their ground-level measurements. With the aid of numerical modeling techniques, future studies could further identify key

39 precursors that drive the rapid formation of formic and isocyanic acids, and
40 quantitatively assess the impacts of the enhanced formation of the two acids aloft on
41 their budgets at ground level.

1. Introduction

Formic acid (HCOOH) is the simplest but the most abundant organic acid in the troposphere. It has been widely measured in aqueous (clouds and aerosols) and gaseous phases over urban, rural, and remote regions *(Kawamura and Kaplan, 1983; Chebbi and Carlier, 1996; Kesselmeier et al., 1998; Yu, 2000)*. As important contributors to the acidity of precipitation, formic and acetic acids can account for 60% of the free acidity in remote regions *(Galloway et al., 1982; Andreae et al., 1988)*, and over 30% of the free acidity in heavily polluted regions *(Keene and Galloway, 1984)*. Formic acid is also an important sink of hydroxyl radicals (OH) in clouds *(Jacob, 1986)*, playing vital roles in modulating the atmospheric aqueous-phase chemistry through changing pH-dependent reaction rates of related constituents. An in-depth understanding of the concentration levels, spatiotemporal variations, and sources of formic acid is key to elucidating the formation mechanisms of atmospheric secondary pollution. However, the sources and sinks of atmospheric formic acid are still poorly understood so far.

There have been many reported sources of atmospheric formic acid. Primary emissions from vegetation activity *(Andreae et al., 1988; Kesselmeier et al., 1998)*, microbial metabolism *(Enders et al., 1992)*, biomass burning *(Goode et al., 2000)*, and vehicle exhaust *(Kawamura et al., 2000)* were identified as important sources of formic acid. Secondary formation from photochemical degradation of volatile organic compounds (VOCs) is another significant source of formic acid *(Khare et al., 1999; Veres et al., 2011; Le Breton et al., 2014; Liggio et al., 2017)*. However, current chemical transport models still highly underestimate ambient concentrations of formic acid *(Stavrakou et al., 2011; Paulot et al., 2011; Millet et al., 2015)* and cannot well reproduce its vertical variations. For example, Mattila et al. *(2018)* measured vertical profiles of formic acid using an elevator on the Colorado Front Range BOA tower. They found that formic acid mixing ratios generally decreased with height throughout the day, but there were no known sources to explicitly explain the net surface emissions. In combination with vertical gradient and flux measurements of formic acid in a forest

ecosystem, Alwe et al. *(2019)* suggested that secondary formation, rather than primary emission, is the major source of ambient formic acid. The vertical distribution and variation patterns of formic acid in the atmospheric boundary layer can provide valuable information on the identification and determination of source contributions. Nevertheless, the vertical variations and key drivers of formic acid, particularly in urban regions, are still unclear due to the lack of adequate vertical observations.

Isocyanic acid (HNCO) is an inorganic acid and has attracted extensive concerns worldwide in recent years due to its strong toxicity *(Wang et al., 2007; Jaisson et al., 2011; Koeth et al., 2013)*. Previous studies have reported that isocyanic acid is highly soluble at physiological pH and the dissociated cyanate ions (NCO^-) are closely linked to atherosclerosis, cataracts, and rheumatoid arthritis *(Mydel et al., 2010; Roberts et al., 2011)*. At present, there is no standard to clearly define the critical levels of isocyanic acid pollution in ambient air *(Rosanka et al., 2020)*. The mixing ratio of HNCO in the atmosphere exceeding 1 ppbv may endanger human health *(Roberts et al., 2011)*, and the protein carbamylation caused by HNCO in human body may induce various risks *(Verbrugge et al., 2015)*. Similar to formic acid, our understanding of isocyanic acid sources is also very limited.

As reported in the literature, primary emissions of isocyanic acid are mainly from combustion sources including cigarette smoke *(Hems et al., 2019)*, gasoline and diesel engine exhausts *(Wren et al., 2018)*, and biomass combustion *(Wentzell et al., 2013; Li et al., 2021; Chandra and Sinha, 2016)*. Wet and dry deposition is known as the main sink of isocyanic acid *(Roberts et al., 2014; Rosanka et al., 2020)*. In addition, isocyanic acid is highly soluble at atmospheric pH and can be hydrolyzed to NH_3 and CO_2 *(Zhao et al., 2014; Roberts and Liu, 2019)*. Secondary formation is another important source of atmospheric isocyanic acid and the known precursors include amides *(Barnes et al., 2010)*, urea *(Jathar et al., 2017)*, and nicotine *(Roberts et al., 2011; Borduas et al., 2016)*. Amides are reported to be the main precursors of isocyanic acid in urban regions *(Wang et al., 2020)*. Isocyanic acid is the oxidative degradation product of amides

initiated by OH radicals, NO_3, radicals, and Cl atoms *(Barnes et al., 2010)*. In addition to primary emissions from organic solvents and various industrial processes, amides can be also formed through the atmospheric accretion reactions of organic acids with amines or ammonia *(Barnes et al., 2010; Yao et al., 2016)*. Vertical gradient measurements of HNCO can help elucidate potential formation sources and mechanisms.

Chemical ionization mass spectrometry (CIMS) can effectively detect and quantify atmospheric formic and isocyanic acids *(Bannan et al., 2014; Chandra and Sinha, 2016; Liggio et al., 2017; Mungall et al., 2018; Fulgham et al., 2019)*. CIMS has been widely used onboard aircraft or on towers to make online vertical measurements of formic and isocyanic acids *(Liggio et al., 2017; Mattila et al., 2018)*. Aircraft can carry many types of instruments and achieve measurements of a large suite of parameters *(Benish et al., 2020; Zhao et al., 2021)*, but the cost is also very expensive. Towers can provide vertical observations of target species by setting up sites at different heights, building mobile platforms (elevators or baskets) *(Mattila et al., 2018)*, and drawing air from multiple heights to the ground-based instruments through long tubes *(Hu et al., 2013; Yáñez-Serrano et al., 2018)*. The usage of long tubes is the most convenient and cost-effective method to make gradient measurements of target gaseous species so far. However, interactions between gaseous species and tubing walls may bring unexpected uncertainties for their measurements *(Helmig et al., 2008a; Helmig et al., 2008b; Schnitzhofer et al., 2009; Karion et al., 2010; Pagonis et al., 2017)*. Therefore, the impacts of long tubing on measurements of formic and isocyanic acids need to be elucidated.

In this study, we first assessed the effects of long perfluoroalkoxy (PFA) Teflon tubes on measurements of formic and isocyanic acids. Vertical gradient measurements of the two acids were made through long tubes on a tall tower in urban Beijing, China. Then, the vertical variations and sources of the two acids were investigated and discussed. At last, key conclusions and implications of this study were summarized.

2. Methods and materials

2.1. Site description and field campaign

Vertical gradient measurements of gaseous species were made on the Beijing Meteorological Tower, which is located on the campus of the Institute of Atmospheric Physics (IAP), Chinese Academy of Sciences. Beijing is the capital city of China with a population of over 20 million by 2020. Beijing has large anthropogenic emission intensities and is suffering from severe air pollution problems *(Acton et al., 2020; Meng et al., 2020; Tan et al., 2022)*. The tower is located in the northern part of downtown Beijing between the 3rd and 4th Ring Roads and is surrounded by urban roads, expressways, residential areas, restaurants, urban landscaping, and parks. As a result, concentrations of the primary pollutants at the tower site are mainly contributed by both anthropogenic (e.g., vehicular exhausts, cooking, and household volatile chemical products) and biogenic emissions. Detailed descriptions of the tower have been provided in previous studies *(Acton et al., 2020; Yan et al., 2021)* and will not be repeated here. The field campaign was carried out from July 17th to August 3rd, 2021.

2.2. Instrumentation

To obtain online gradient measurements of atmospheric trace gases, we established a tower-based observation system using a combination of online measurement techniques and long tubes (Figure S1). The system and related assessments on the usage of long tubes have been explicitly described in our previous study *(Li et al., 2023)* and will be briefly introduced here. After removing fine particles by PFA Teflon filters (Whatman) with a diameter of 46.2 mm and a pore size of 2 μm, ambient air at four altitudes on the tower (namely 47, 102, 200, and 320 m) was simultaneously and continuously drawn to the ground through long PFA Teflon tubes (100, 150, 250, and 400 m; outer diameter: 1/2"; inner diameter: 0.374") by a vacuum pump. All the sampling tubes were installed inside the iron tower to avoid direct sunlight. The flow rate of the sample stream in each tube was controlled by a critical

orifice and ranged between 13-21 standard liters per minute (SLPM), as shown in table S1. The flow rates in long tubes were retained as large as possible if instruments allowed to minimize the impact of gas-surface interactions on measurements of targeted gaseous species *(Deming et al., 2019; Li et al., 2023)*. Two air-conditioned containers were placed next to each other on the base of the tower and all the instruments were operated inside. An additional inlet of the tube was mounted on the rooftop of the container (approximately 5 m above ground level) to make measurements of trace gases near the surface. Therefore, the tower-based observation system consisted of five inlet heights ranging from the ground level to 320 m. Inlets of the instruments were connected to the outlet of a Teflon solenoid valve group, which was used to perform the switch of the inlet heights at time intervals of 4 minutes. Vertical gradient measurements of gaseous species were cyclically made over periods of 20 minutes. Indoor PFA Teflon tubes were wrapped with insulation tubes and were heated to prevent condensation of water and organic gases.

Formic and isocyanic acids were measured by a high-resolution time-of-flight chemical ionization mass spectrometry with iodide reagent ion (ToF-CIMS). Due to the high sensitivity to oxygenated volatile organic compounds (OVOCs), the iodine ion source has been widely used in previous studies *(Yuan et al., 2015; Schobesberger et al., 2016; Mungall et al., 2018)*. A Filter Inlet for Gases and AEROsols (FIGAERO) was used to perform the switch between the gas and particle measurement modes *(Lopez-Hilfiker et al., 2014)*. The ion molecular reaction (IMR) chamber is adjacent to the FIGAERO and utilizes a vacuum ultraviolet ion source (VUV-IS). Iodide anion (I^-) is produced from the photoionization of methyl iodide (CH_3I) in IMR *(Ji et al., 2020)*. During the measurements, I^- was produced by introducing the CH_3I gas standard (1000 ppm, Dalian Special Gases, China) to the IMR chamber at a flow rate of 2 standard cubic centimeters per minute (SCCM) in 200 SCCM high-purity nitrogen (N_2, 99.9995%) by the VUV-IS. The pressure of the IMR chamber was maintained at 70-80 mbar. Flow rates of the sample gas were maintained at 2 SLPM using a critical orifice.

During the field campaign, both gaseous and particle measurements were made through the FIGAERO of the CIMS, but only gaseous measurements were analyzed in this study. In a one-hour cycle, the first 24 min was allocated to make gaseous measurements during which a complete vertical profile of a gaseous species can be obtained. As shown in Figure S3, there was no significant difference between the background signals of the instrument made with and without the long tubes. Therefore, blank measurements of the instrument were made by adding zero air just to the inlet of the instrument without through the long tubes during the field campaign. In the gaseous measurement mode, a rapid blank measurement was made for 10 s at 3-min intervals in the first 21 min and a long-time blank measurement was made in the rest 3 min *(Palm et al., 2019)*. During the first 21-min period of the one-hour cycle, another inlet at 5 m was used to collect ambient particles using PTFE membrane filters (Zefluor®, Pall Inc., USA). Therefore, the remaining 36 min of the one-hour cycle was allocated to analyze the collected particle.

Calibrations of the ToF-CIMS for formic and isocyanic acids were performed in the laboratory before and after the field campaign. Standard solutions of formic acid were evaporated using the liquid calibration unit (LCU, IONICON Analytik GmbH) and then diluted to designated concentration gradients by being mixed with zero air at five flow rates. The gas standard of isocyanic acid is unstable at ambient temperature and thus no commercial gas cylinder was available. Instead, cyanuric acid solution was put into a diffusion cell and heated to 300 ˚C to generate isocyanic acid gas at a stable mixing ratio. An ion chromatograph was used to quantify the concentration of the gas standard by measuring deionized water that absorbed the isocyanic acid gas. Detailed information about the isocyanic acid calibration procedure has been provided in our previous work *(Wang et al., 2020)*. Impacts of the changes in ambient humidity on measurements of the ToF-CIMS for both formic and isocyanic acids were determined in the laboratory and were corrected when calculating their respective concentrations. Measured signals of the ToF-CIMS were processed using the Tofware software package

(version 3.0.3; Tofwerk AG, Switzerland).

A high-resolution proton-transfer-reaction quadrupole interface time-of-flight mass spectrometry (PTR-ToF-MS) with both H_3O^+ and NO^+ ion chemistry was used to measure reported precursors of the two acids, such as isoprene, aromatics, OVOCs, and amides. Detailed information about the configuration and operation setup of the PTR-ToF-MS has been provided in our previous studies *(Yuan et al., 2017; Wu et al., 2020; Li et al., 2022)*. Mixing ratios of O_3, CO, and NO_2 were measured by a UV absorption O_3 analyzer (T400, Teledyne API, USA), a gas filter correlation CO analyzer (T300, Teledyne API, USA), and a trace level NOx analyzer (42i, Thermos, USA), respectively. Photolysis rates were measured by a PFS-100 photolysis spectrometer (Focused Photonics Inc.) on the rooftop of the container. The planetary boundary layer height (PBLH) data was obtained from the web portal of the Real-time Environmental Applications and Display sYstem (READY) of the National Oceanic and Atmospheric Administration (NOAA) Air Resource Laboratory (https://ready.arl.noaa.gov/READYamet.php). Measurements of isocyanic acid and amides made in Guangzhou and Gucheng in China were also used in this study for comparison, and more information about these observations can be found in our previous papers *(Wang et al., 2020)*.

2.3. Tubing assessment

The tower-based observation system used long PFA Teflon tubes (hundreds of meters in length) to draw air samples from different heights. The interactions between tubing inner walls and organic compounds, namely the absorption/desorption of trace gases, have nonnegligible impacts on their measurements after traversing such long tubes *(Pagonis et al., 2017; Deming et al., 2019)*. The equilibrium between the absorption and desorption of organic compounds on tubing walls required distinct times, namely tubing delay, for different species. For nonpolar/weak-polar organic compounds, their tubing delays and measurement uncertainties after traversing long tubes are dependent on their saturation concentrations and the flow rates of sample streams but

are independent of changes in humidity *(Krechmer et al., 2017; Pagonis et al., 2017)*. For some small polar organic compounds, their tubing delays and measurement uncertainties after traversing long tubes are dependent on Henry's law coefficients and are affected by changes in humidity *(Liu et al., 2019)*. The performance of long PFA Teflon tubes in measuring concentrations of nonpolar/weak-polar organic compounds and inorganic species (e.g., ozone, NO, NO_2, and CO_2) has been assessed in our previous work *(Li et al., 2023)*. The impacts of long PFA Teflon tubes on measurements of formic and isocyanic acids are still unclear and will be assessed in this study.

Long PFA Teflon tubes with an outer diameter of 1/2" and an inner diameter of 0.374" were used to draw air samples from different altitudes and thus were assessed. At flow rates below 20 SLPM, suitable pressure drops can be maintained in these long tubes for instrument operation *(Li et al., 2023)*. The effects of long tubes on measurements of formic and isocyanic acids were mainly assessed using the same methods in the literature *(Li et al., 2023)*. The tubing delay of formic acid is estimated as the time required to reach 90% of the concentration change made at the tubing inlet. The depassivation curve of formic acid measured at the outlet end of the long tubing was used to calculate its tubing delay and was obtained by using a step-function change of the formic acid concentration from 7.5 ppbv to 0 ppbv at the tubing inlet *(Pagonis et al., 2017; Deming et al., 2019)*. The formic acid signals were normalized to those measured at the beginning of the step-function change and then were fitted using the double exponential method, as shown in Figure 1. Finally, the tubing delay of formic acid was determined when the fitting line decreased to 0.1. The previous study *(Li et al., 2023)* has reported that inorganic species have small tubing delays even in a 400 m long tube. Therefore, tubing delays of isocyanic acid in long tubes are not discussed in this study.

To further assess the impacts of long tubes (namely 100, 200, 300, and 400 m) on measurements of formic and isocyanic acids in real environments, their ambient mixing ratios measured through different lengths of tubes were intercompared by

running the inlets side by side at ground level. Ambient air samples were sequentially drawn with and without the tubes through a Teflon solenoid valve group (Figure S2), which was set to perform the switch at time intervals of 4 minutes. Instrument backgrounds of the two species were measured for 10 s at time intervals of 1 minute by passing zero air into the instrument at a flow rate of 3 SLPM. Inter-comparisons of the formic acid and isocyanic acid measurements made through different lengths of tubes were mainly performed using linear fittings ($y=kx+b$; k is the slope and b is the intercept).

3. Results and Discussions

3.1. Interactions between long tubes and the two acids

As shown in Figure 1, signals of formic acid measured by the ToF-CIMS had a tubing delay of 23 s after traversing the 400 m long tube at the flow rate of 13 SLPM. In addition to the interactions between tubing walls and formic acid molecules *(Pagonis et al., 2017; Deming et al., 2019)*, molecular diffusion and dispersion (namely Taylor dispersion) can cause the longitudinal mixing of gas molecules in the tubing and is also an important factor contributing to the measured delays *(Karion et al., 2010)*. Molecular diffusion and dispersion have strong dependences on molecular diffusion coefficients and tubing flow rates *(Karion et al., 2010)*. The influential time of Taylor dispersion on the measurements of formic acid through a 400 m long tube at the flow rate of 13 SLPM was estimated to be only 2.9 s, which is much smaller than the measured tubing delay (23 s) of formic acid. Therefore, the adsorption/desorption of formic acid molecules on tubing inner walls plays a dominant role in determining the tubing delay.

For most organic compounds, the tubing delays generally depend on tubing flow rates and their saturated concentrations (C^*) *(Li et al., 2023; Deming et al., 2019)*. With the increase in tubing length and flow rate, the tubing delays of organic compounds will rapidly decrease *(Liu et al., 2019)*. Therefore, the tubing flow rates should be as large as possible if the instrument could work normally. In addition, the tubing delays of

organic compounds generally increase with the decrease in their *C* (Li et al., 2023)*. It must be acknowledged that tubing delay is inevitable. The analysis time scales of species concentrations measured through long tubes should be greater than their tubing delays, especially for those with small *C**.

The delay time of formic acid mentioned here is different from the residence time of the gas through the long tubing. Residence time refers to the time required for the sample gas to pass through the tubes. As for the measured tubing delays of trace gases, they refer to the amounts of time required for the instruments to measure stable concentrations of targeted species in response to a change in species concentrations at the tubing inlet. The residence time is the same for all trace gases, depending on the length of the long tube, the inner diameter of the tube, and the flow rate of the sample gas. However, the tubing delay for each trace gas is different and depends on the flow rate, their respective saturated concentrations/Henry's constants, and molecular diffusion and diffusion rates. The difference between residence time and delay time is also discussed in detail in our previous work *(Li et al., 2023)*.

As shown in Figure S4(a), ambient mixing ratios of formic acid measured through the 400 m long tube varied consistently with those measured without the tube with mean values of 4.14 and 4.09 ppbv, respectively. The mixing ratios of formic acid measured with the long tube were slightly higher in the daytime and lower at night in comparison with those measured without the long tube. We also conducted a correlation analysis between the mixing ratios of formic acid measured with and without long tubes. As shown in Figure 2, the mixing ratios of formic acid measured with and without the 400 m long tube agreed within 20%, but the slope of the linear fitting (k=0.84) is lower than 1. The differences of formic acid mixing ratios measured with and without the 400 m long tube were predominantly caused by the long-tail memory effect of the tubing (Figure 1). For example, the mixing ratios of formic acid measured through the 400 m long tube at night equaled to its ambient mixing ratios plus those released from the tubing inner wall. The tubing delay of formic acid was determined when its mixing

ratios reached 90% of the change before entering the tubing. However, the long-tail memory effect of the tubing mainly focused on the rest 10% of the change (Figure 1), which required a much longer time to stabilize.

Impacts of the tubing memory effects will be accumulated due to the continuous change in ambient concentrations of formic acid. To further assess the impacts of tubing memory effects on measurement uncertainties of the two acids, differences between mixing ratios of the species X (namely formic and isocyanic acids) measured with and without long tubes at time *t* (denoted by $\delta[X]_t$) were calculated using Eq. (1):

$$\delta[X]_t = [X_{without}]_t - [X_{with}]_t \quad (1)$$

where $[X_{with}]_t$ and $[X_{without}]_t$ refer to mixing ratios of the species X measured at time *t* with and without long tubes, respectively. In addition, the changes in mixing ratios of the species X measured using long tubes was also calculated using Eq. (2):

$$\Delta[X]_t = [X_{with}]_t - \frac{\sum_{t-\Delta t}^{t}[X_{with}]}{\Delta t} \quad (2)$$

where Δt is the change in time relative to time *t* and was used to characterize the influential time of the memory effect. A strong correlation between $\delta[X]_t$ and $\Delta[X]_t$ could be captured at a certain Δt if the tubing memory effect make essential contributions to measurement uncertainties of the species X after traversing long tubes. For the 400 m long tubing, $\delta[X]_t$ and $\Delta[X]_t$ had the strongest correlation (R^2=0.89) when Δt was approximately 14 h (Figure S7). As also shown in Figure 2(a), the mixing ratios of formic acid measured with and without the 400 m long tube agreed well when $\Delta[HCOOH]$ approached to zero. The decrease and increase in $\Delta[HCOOH]$ will enlarge measurement uncertainties of formic acid using the long tube. In morning periods, ambient mixing ratios of formic acid rapidly increased. As a result, the mixing ratios of formic acid measured through the 400 m long tube were slightly lower than its ambient mixing ratios due to the absorption of formic acid by tubing inner walls. In evening and nighttime periods, an opposite phenomenon was observed due to the desorption of formic acid from tubing inner walls (Figure S4).

In addition to the 400 m long tube, impacts of the tubes with lengths of 100, 200,

and 300 m on measurements of formic acid were also assessed, as shown in Figures 2(c) and 3(a). The usage of tubes with lengths of 100, 200, and 300 m has negligible impacts on the measurements of formic acid. During the test of the 200 m tubing, meteorological conditions significantly changed with lower temperatures and stronger winds in comparison to the days on which the tests of the other lengths of tubes were performed. As shown in Figure S5, the concentrations of formic acid and isocyanic acid were evidently enhanced and significantly varied during the 400 m tubing test. In contrast, ambient concentrations of formic and isocyanic acid were relatively low and slightly varied, resulting in the exceedingly large or low values of k and R^2 between the concentrations of formic acid measured with and without the 200 m long tubing. However, according to the results of the test, the average concentration difference of formic and isocyanic acid measured with and without the 200 m tubing agreed well within 4%, suggesting that the 200 m long tube has minor effects on the measurements of formic and isocyanic acid.

In contrast to formic acid, the usage of long tubes had minor impacts on the measurements of isocyanic acid. The mixing ratios of isocyanic acid measured with and without the 400 m long tube varied consistently (k=0.86, R^2=0.90) with mean values of 0.25 and 0.26 ppbv, respectively (Figure S4). As shown in Figure 2(b), $\Delta[HNCO]$ is evenly distributed on both sides of the 1:1 line. Therefore, the changes in ambient concentrations of isocyanic acid do not have significant impacts on the measurements of isocyanic acid through the long tubes. As also shown in Figure 3(b), $\delta[HNCO]$ and $\Delta[HNCO]$ of isocyanic acid were independent of the changes in isocyanic acid mixing ratios. The R^2 values of linear fittings were less than 0.21 for the isocyanic acid measurements made using different lengths of tubes. This is consistent with the results reported in the literature *(Helmig et al., 2008a; Helmig et al., 2008b; Li et al., 2023)* that inorganic species with low reactivities can be well measured using long PFA Teflon tubes. The test results confirmed that the measurements of formic acid and isocyanic acid through long tubes can be used to characterize their vertical and temporal

variability. However, a further correction of the formic acid measurements made through the long tubes must be performed if they were used to accurately calculate the kinetic parameters of chemical reactions regarding the formation and removal of formic acid at different heights.

3.2. Vertical variations and sources of formic acid

Time series of formic acid and ozone mixing ratios at 5 and 320 m are shown in Figure 4. The concentrations of formic acid and ozone exhibited similar diurnal and inter-diurnal variations at different altitudes during the campaign. Hourly mean mixing ratios of ozone exhibited strong temporal variations with an average of 43.5±25.3 ppbv at 5 m and an average of 53.5±25.0 ppbv at 320 m. Hourly mean mixing ratios of formic acid at 5 m ranged between 0.1-6.6 ppbv with an average of 1.3±1.3 ppbv at 5 m, which is comparable to those observed in other megacities, such as Shenzhen (1.2 ppbv) in China *(Zhu et al., 2019)*, London (1.3 ppbv) in UK *(Bannan et al., 2017)*, and Los Angeles (2.0 ppbv) in USA *(Yuan et al., 2015)*. By contrast, hourly mean mixing ratios of formic acid at 320 m had an average of 2.1±1.9 ppbv, approximately 1.6 times higher than that at 5 m. The temporal variability of formic and isocyanic acids were mainly caused by the diurnal and inter-diurnal changes in meteorological conditions (e.g., solar radiation and PBLH).

Before July 12th, the daily maximum hourly mixing ratios of ozone at 5 m all exceeded 100 ppbv, indicating the enhanced formation of secondary air pollutants associated with photochemical reactions. The mixing ratios of formic acid measured before July 12th were also prominently larger than those measured after, suggesting important contributions from photochemical formations. The photochemical formation of secondary pollutants was weak from July 13th to 30th due to the cloudy and rainy weather. After August 1st, low mixing ratios of ozone and formic acids were observed along with the occurrence of favorable dilution conditions characterized by high PBLHs.

As shown in Figure 5, the mixing ratios of formic acid measured at the five altitudes (namely 5, 47, 102, 200, and 320 m) exhibited similar diurnal patterns. After

sunrise (~6:00 LT), formic acid mixing ratios increased rapidly at each altitude before reaching the peak between 14:00-16:00 LT and then continuously declined before sunrise the following day. Similar diurnal variation patterns of formic acid were also observed at other urban sites *(Veres et al., 2011)*, rural sites *(Hu et al., 2022)*, and remote sites *(Schobesberger et al., 2016)*. The diurnal variation patterns of formic acid were highly similar to those of ozone (a typical secondary pollutant) but were different from those of VOCs from primary emissions. Taking toluene as an example, toluene is a typical VOC tracer of anthropogenic emission sources in urban regions, such as industrial processes and vehicular exhausts *(Fang et al., 2016; Skorokhod et al., 2017)*, and is also an important precursor of ozone *(Yuan et al., 2012)*. The mixing ratios of toluene exhibited opposite diurnal variation patterns to those of ozone and formic acids with the minima occurring at around 14:00 LT. The lower mixing ratios of toluene in daytime than in nighttime were predominantly caused by the enhancement of atmospheric dilution and chemical removal by OH radicals *(De Gouw et al., 2018)*. The mixing ratios of formic acid poorly correlated (R^2 ranged between 0.16-0.28) with those of CO (a typical tracer of combustion sources) at the five altitudes but well correlated (R^2 ranged between 0.67-0.75) with those of Ox (O_3+NO_2, a conserved metric of ozone by removing NO titration effect), as shown in Figure 6. These results further confirm that ambient concentrations of formic acid in urban Beijing were dominantly contributed by secondary sources associated with photochemical reactions rather than primary emissions.

Another observed evidence for the dominant contribution of formic acid from secondary formations is its positive vertical gradients in nighttime (defined as the period of 22:00-5:00 LT), as shown in Figure 7. Large amounts of formic acid will accumulate near the surface with strong negative vertical gradients if primary emissions dominate its contributions, as manifested by vertical toluene profiles. At nighttime, the mixing ratios of ozone also increased with height due to enhanced removal by NO titration and surface dry deposition. The deposition of formic acid was also enhanced

near the surface, driving the formation of positive gradients in vertical formic acid profiles.

A notable difference existed between the diurnal variation patterns of ozone and formic acid above the ground. As shown in Figure 5, the mean mixing ratios of ozone at 5 m rapidly increased from 21.5 ppbv to 36.0 ppbv from 6:00 to 10:00 LT, while the mean mixing ratios of ozone at 320 m slightly increased from 16.3 ppbv to 16.9 ppbv during the same period. The enhancement rate is defined as the average change rate of the species concentration between two adjacent hours. As shown in Figure 8, the enhancement rates of ozone mixing ratios between 6:00 and 10:00 LT decreased with the increase in height. This phenomenon indicates relatively weak photochemical ozone formation in urban regions aloft before 10:00 LT due to the lack of reactive ozone precursors (e.g., unsaturated hydrocarbons and NOx). With the enhancement of the vertical exchange of air masses with the rise of the boundary layer, large amounts of ozone precursors (e.g., the observed peaks of toluene mixing ratios at 320 m at 10:00 LT) emitted from surface sources were transported upward and drove the formation of ozone in high altitudes. In contrast to ozone, the mixing ratios of formic acid at the five altitudes all increased rapidly between 6:00 and 10:00 LT. The enhancement rate of formic acid mixing ratios between 6:00 and 10:00 LT kept nearly constant below 320 m (Figure 8). This result implies that the oxidation products of VOCs over nighttime or in the daytime before are important precursors of formic acid and can drive the rapid formation of formic acid with further photooxidation. This speculation can be supported by the vertical and diurnal variations of methyl vinyl ketone (MVK), methacrolein (MACR), and formaldehyde, which are reported key precursors of formic acid as shown in Figure 5(d) and 5(e). The diurnal variation patterns of MVK+MACR and formaldehyde at the five latitudes were nearly the same with the enhancements in daytime. In addition, concentrations of MVK+MACR and formaldehyde all increased with height in nighttime and early morning periods, facilitating the photochemical formation of formic acid even in the residual layer.

As a reactive hydrocarbon species, the mixing ratios of toluene rapidly decreased with height in daytime (defined as the period of 11:00-16:00 LT, as shown in Figure 7) due to the combined effects of atmospheric dilution and OH-initiated chemical removal. By contrast, the mixing ratios of ozone and formic acid increased with height. The mixing ratios of ozone and formic acid all rapidly increased with height below 102 m, predominantly attributed to the reduced effect of surface dry deposition with the increase in height. The mean mixing ratios of formic acid increased by 18% from 102 m to 320 m in daytime, while ozone mixing ratios were well mixed above 102 m. Our results point to the likely importance of photochemistry as a source of formic acid that is enhanced with increasing height within the boundary layer.

The precursors and formation mechanisms of atmospheric formic acid have been extensively investigated in previous studies but still remain uncertain. Isoprene has long been recognized as an important precursor of formic acid through reactions with O_3 and OH radicals *(Neeb et al., 1997; Paulot et al., 2009)*. Recent studies also found that the degradation of organic aerosols (OA) derived from isoprene is an important source of formic acid *(Cope et al., 2021; Bates et al., 2023)*. In addition, the photooxidation of other biogenic and anthropogenic hydrocarbons is also a key source of formic acid *(Paulot et al., 2011; Millet et al., 2015; Link et al., 2021)*. Figure 9 illustrates the mean vertical profiles of several key precursors of formic acid in daytime. The concentrations of isoprene and toluene (Figure 7) all decreased rapidly with height. By contrast, MVK and MACR, the primary oxidation products of isoprene *(Grosjean et al., 1993)*, exhibited weak vertical gradients. Formaldehyde, a more general photooxidation product of VOCs, exhibited similar vertical distribution patterns to those of ozone. Large amounts of OVOCs were produced and accumulated in higher altitudes through the oxidation of hydrocarbons and the further oxidation of some OVOCs during their upward mixing course. MVK, MACR, and formaldehyde are also key precursors of formic acid. MVK and MACR can react with O_3 to produce formic acid *(Link et al., 2020)*. Formaldehyde can be converted to methanediol in cloud droplets and then be

488 rapidly oxidized by OH to produce formic acid *(Franco et al., 2021)*. In addition, enol
489 *(Lei et al., 2020)* and many other OVOCs (such as glycolaldehyde *(Butkovskaya et al.,*
490 *2006a)* and hydroxyacetone *(Butkovskaya et al., 2006b)* can be further oxidized to
491 produce formic acid. Therefore, high concentrations of OVOCs aloft may be the
492 dominant factor that largely enhances the photochemical formation of formic acid in
493 urban regions.

494 As discussed above, formic acid exhibited strong positive vertical gradients
495 throughout the day, implying that the concentrations of formic acid measured at ground
496 level were not capable of accurately characterizing its abundance and temporal
497 variability in the whole boundary layer. Besides, the formic acid formed in daytime and
498 retained in the nocturnal residual layer also has vital impacts on the budget of formic
499 acid in the boundary layer. Thus, we used the column-integrated concentration (CIC)
500 of formic acid (the sum of the abundance in both the nocturnal residual layer and the
501 boundary layer, see detailed definitions in SI) to further clarify the diurnal variability
502 in the abundance of formic acid in the boundary layer.

503 As shown in Figure 10, the CICs of formic acid had a flatter diurnal pattern in
504 comparison to those at ground level. The CICs of formic acid had approximately stable
505 values overnight and reached a maximum at 16:00 LT. The ratio of the maximum and
506 minimum of CIC for formic acid was only 1.3, while it was 4.2 for the concentrations
507 of formic acid at 5 m. The ground-level measurements were more affected by
508 depositional losses, while such depositional losses in the residual layer were nearly
509 absent. However, the chemical species retained in the residual layer were closely related
510 to their budgets in the daytime boundary layer. If the removal rates of formic acid from
511 ground-level measurements were used to characterize those at high altitudes (e.g., in
512 the residual layer), the removal of formic acid in the entire boundary layer would be
513 overestimated. As the result, numerical models cannot accurately reproduce the
514 abundances and budgets of formic acid without the constraints of vertical observations
515 and the clarification of formic acid formation mechanisms.

3.3. Vertical variations and sources of isocyanic acid

The mixing ratios of isocyanic acid also exhibited strong temporal variations during the campaign with a mean of 0.28±0.16 ppbv at 5 m and a mean of 0.43±0.21 ppbv at 320 m, as shown in Figure 11. The mixing ratios of isocyanic acid measured at the ground level in urban Beijing were approximately 10 times higher than those measured in Los Angeles, USA (0.025 ppbv) *(Roberts et al., 2014)* and Calgary, Canada (0.036 ppbv) *(Woodward-Massey et al., 2014)* but were lower than those measured in other regions in China. For example, the mean mixing ratio of isocyanic acid was 0.37 ppbv at a rural site (Gucheng) in the North China Plain (NCP), and 0.46 ppbv in urban Guangzhou in the Pearl River Delta (PRD) region *(Wang et al., 2020)*. Isocyanic acid will pose a threat to human health when its ambient mixing ratios exceed 1.0 ppbv. In this study, isocyanic acid mixing ratios greater than 1.0 ppbv were not observed at ground level but were observed at 320 m on three days. The maximum hourly mixing ratios of isocyanic acid at 320 m reached 1.63 ppbv at 16:00 LT on July 8th.

The mixing ratios of isocyanic acid at the five altitudes exhibited similar diurnal variation patterns. After sunrise, the mixing ratios of isocyanic acid at the five altitudes all simultaneously increased and peaked at about 14:00 LT. Then, isocyanic acid mixing ratios decreased slowly and reached the minimum before sunrise the following day. This diurnal variation pattern of isocyanic acid measured at the ground level in urban Beijing was not consistent with those measured at the Gucheng site in NCP *(Wang et al., 2020)*. The isocyanic acid mixing ratios at the Gucheng site exhibited insignificant diurnal variability throughout the day with only a weak morning peak, predominantly attributed to the enhancement of primary emissions. However, the diurnal variation patterns of isocyanic acid measured at the five altitudes were well correlated with the change in solar irradiance and were consistent with those measured at the two sites in PRD. These results imply that ambient concentrations of isocyanic acid in urban Beijing were mainly contributed by secondary sources associated with photochemical reactions.

Similar to formic acid, the simultaneous increase of isocyanic acid mixing ratios

at the five altitudes with the onset of sunlight also indicates the presence of adequate precursors even in the nocturnal residual layer. In addition, the diurnal variability of isocyanic acid mixing ratios measured below 200 m was much weaker than those measured at 320 m. For example, the ratio of the daily maximum to the daily minimum mixing ratios of isocyanic acid was 1.9 at 320 m, while the ratio was only 1.4 at 5 m. The mean enhancement rate of isocyanic acid mixing ratios at 320 m (0.05 ppbv h^{-1}) between 6:00 and 10:00 LT was approximately five times larger than that at 5 m (0.01 ppbv h^{-1}). The vertical gradients of isocyanic acid between 102 and 320 m were also larger than those below (Figure 12). The rapid increase in both concentrations and enhancement rates of isocyanic acid with height (Figures 8 and 12) implies the enhanced photochemical formation of isocyanic acid in the middle and upper part of the boundary layer.

Secondary formation precursors of atmospheric isocyanic acid were still poorly understood so far. Amides were considered important precursors of isocyanic acid *(Roberts et al., 2014; Rosanka et al., 2020)*. As reported in our previous study *(Wang et al., 2020)*, C_3 amides accounted for the largest fraction of the total concentrations of amides and were dominant contributors to the secondary formation of isocyanic acid. The mixing ratios of C_3 amides in Guangzhou in PRD exhibited strong diurnal variations. Along with the sunrise, the mixing ratios of C_3 amides rapidly decreased and reached the minimum at 13:00 LT. Afterward, the mixing ratios of C_3 amides started to increase and accumulated at night. As shown in Figure S6, the influence of long tubing on the measurement of amides was limited, so we also measured the amides during the field campaign. However, the mixing ratios of C_3 amides in Beijing and Gucheng in NCP exhibited insignificant diurnal variability, consistent with those of isocyanic acid. The mean mixing ratios of C_3 amides at 5 m in urban Beijing is only 0.03 ppbv during the campaign, which is one order of magnitude lower than those in Guangzhou (0.35 ppbv) and Gucheng (0.18 ppbv). The mixing ratios of C_3 amides measured at the five altitudes in urban Beijing were also approximately one order of magnitude lower than

572 those of isocyanic acid (Figure 12). Besides, the mixing ratios of C_3 amides decreased
573 with height in both nighttime and daytime, indicating predominant contributions from
574 primary emissions. This is consistent with the fact that primary emissions of chemical
575 composition from industry-related sources have been largely reduced with the outward
576 migration of industry in urban Beijing. By contrast, the mixing ratios of isocyanic acid
577 increased with height in both day and night with an average of 0.32 ppbv at 5 m and
578 0.60 ppbv at 320 m. These results suggest that C_3 amides were far more enough to
579 account for the secondary formation of isocyanic acid in urban Beijing.

580 Figure 13(a) gives the composition and average concentrations of C_1-C_{10} amides
581 measured at the five altitudes during the campaign. C_2 amides accounted for the largest
582 fraction of the total mixing ratios of amides. The total mixing ratios of amides exhibited
583 decreasing tendencies with the increase in height, suggesting predominant contributions
584 from direct emissions of surface sources. As for formamide, its mixing ratios exhibited
585 an increasing tendency from 0.024 ppbv at 5 m to 0.030 ppbv at 320 m. The positive
586 vertical gradients of formamide suggest its enhanced formation with height, probably
587 due to the enhancements of formic acid. However, the average concentration ratios of
588 formamide to formic acid slightly varied between 0.01 and 0.02 among the five heights.
589 The average concentration ratios of formamide to isocyanic acid decreased from 0.09
590 at 5 m to 0.07 at 320 m. These results imply that the formation of isocyanic acid through
591 the pathway of HCOOH-CH_3NO-HNCO may be enhanced with the increase in height
592 but could only contribute a tiny fraction of the observed isocyanic acid, as shown in
593 Figure 13(b). Assuming the full conversion of C_1-C_{10} amides to isocyanic acid, the
594 average concentration ratios of amides (sum of C_1-C_{10}) to isocyanic acid below 320 m
595 only ranged between 0.32 and 0.56 and decreased with height. Therefore, in addition to
596 amides, there must be other important precursors and formation pathways of isocyanic
597 acid, particularly in high altitudes. The simultaneous increase of isocyanic acid
598 concentrations at the five heights upon sunrise (Figure 11) implies the presence of
599 adequate precursors in the nocturnal residual layer. The oxidation products of VOCs

driven by ozone and NO_3 radicals in nighttime may be an important class of precursors. In addition, the largest enhancement rates and highest concentrations of isocyanic acid at 320 m in daytime also suggest that high concentrations of OVOCs and low-NOx conditions may enhance the secondary formation of isocyanic acid.

The positive vertical gradients of isocyanic acid imply that the secondary formation of isocyanic acid aloft could serve as an important source of surface isocyanic acid in daytime driven by turbulence mixing. The CICs of isocyanic acid were calculated to further clarify its abundance and temporal variability in the whole boundary layer. Distinct diurnal patterns were observed between the ground-level concentrations and CICs of isocyanic acid. Analogous to formic acid, the CICs of isocyanic acid varied insignificantly over nighttime and enhanced in daytime, reaching the maximum at approximately 14:00 LT. The formation of some chemicals can be largely enhanced at higher altitudes and so using ground-level measurements to constrain numerical models may be not adequate.

4. Conclusion

In this study, vertical and diurnal variations of formic and isocyanic acids in urban Beijing were investigated using tower-based online gradient measurements. The measurements of isocyanic acid can be well measured through long PFA Teflon tubes. The measurements of formic acid made through long tubes were slightly influenced by the memory effect of tubing walls, and the vertical increasing gradients of formic acid may be slightly enhanced if the tubing effects were considered. The concentrations of formic and isocyanic acids all increased with height in both nighttime and daytime. The diurnal and vertical distribution patterns of formic and isocyanic acids all suggest that their abundances in the boundary layer were dominantly contributed by secondary formation associated with photochemical reactions. The photochemical formations of formic and isocyanic acids were also substantially enhanced with the increase in height. The formation pathway of isocyanic acid through HCOOH-CH_3NO-HNCO only

accounted for a tiny fraction of its ambient abundance. The formic and isocyanic acids photochemically formed in the middle and upper parts of the boundary layer were important sources for those at ground level in urban region. The differences of the diurnal patterns between CICs and ground-level concentrations of formic and isocyanic acids further highlight the importance of vertical observations in elucidating their budgets and sources in the whole boundary layer.

Characterization of the vertical variations in formic and isocyanic acids could provide valuable information for elucidating their budgets and sources in the boundary layer. However, there are still many important but unresolved questions associated with the vertical distributions of formic and isocyanic acids. For example, the key precursors that drive the rapid formation of formic and isocyanic acids in the residual layer are still unknown. Are there any changes in the key precursors and formation pathways of formic and isocyanic acids with the increase of height in urban region? To answer these questions, the combination of vertical gradient measurements of more chemical species and numerical simulations is needed in future studies.

Supporting Information: Additional experimental details, materials, and methods, including schematic illustration of tubing test, determination of the long tubes' cumulative influence, and calculation of CICs.

Data availability

Data related to this article are available online at https://doi.org/10.7910/DVN/ANH0WE.

Author contributions

QY, XBL, BY, and YH designed the research. QY, XBL, BY, XZ, YH, LY, XH, JQ and MS contributed to the data collection and data analysis. QY and XBL wrote the paper with contributions from all coauthors. All the coauthors discussed the results and reviewed the paper.

Competing interests

The authors declare that they have no conflict of interest.

Acknowledgment

This work was financially supported by the National Key R&D Plan of China (grant No. 2023YFC3706103, 2023YFC3706201, 2022YFC3700604) and the National Natural Science Foundation of China (grant No. 42121004, 42275103, 42205094, 42230701, 42305095). This work was also supported by the Special Fund Project for Science and Technology Innovation Strategy of Guangdong Province (Grant No. 2019B121205004). The authors would like to thank the personnel who participated in data collection, instrument maintenance, and logistic support during the field campaign.

Reference

Acton, W. J. F., Huang, Z., Davison, B., Drysdale, W. S., Fu, P., Hollaway, M., Langford, B., Lee, J., Liu, Y., Metzger, S., Mullinger, N., Nemitz, E., Reeves, C. E., Squires, F. A., Vaughan, A. R., Wang, X., Wang, Z., Wild, O., Zhang, Q., Zhang, Y., and Hewitt, C. N.: Surface–atmosphere fluxes of volatile organic compounds in Beijing, Atmospheric Chemistry and Physics, 20, 15101-15125, 10.5194/acp-20-15101-2020, 2020.

Alwe, H. D., Millet, D. B., Chen, X., Raff, J. D., Payne, Z. C., and Fledderman, K.: Oxidation of Volatile Organic Compounds as the Major Source of Formic Acid in a Mixed Forest Canopy, Geophysical Research Letters, 46, 2940-2948, https://doi.org/10.1029/2018GL081526, 2019.

Andreae, M. O., Talbot, R. W., Andreae, T. W., and Harriss, R. C.: Formic and acetic acid over the central Amazon region, Brazil: 1. Dry season, Journal of Geophysical Research: Atmospheres, 93, 1616-1624, https://doi.org/10.1029/JD093iD02p01616, 1988.

Bannan, T. J., Bacak, A., Muller, J. B. A., Booth, A. M., Jones, B., Le Breton, M., Leather, K. E., Ghalaieny, M., Xiao, P., Shallcross, D. E., and Percival, C. J.: Importance of direct anthropogenic emissions of formic acid measured by a chemical ionisation mass spectrometer (CIMS) during the Winter ClearfLo Campaign in London, January 2012, Atmospheric Environment, 83, 301-310, 10.1016/j.atmosenv.2013.10.029, 2014.

Bannan, T. J., Murray Booth, A., Le Breton, M., Bacak, A., Muller, J. B. A., Leather, K. E., Khan, M. A. H., Lee, J. D., Dunmore, R. E., Hopkins, J. R., Fleming, Z. L., Sheps, L., Taatjes, C. A., Shallcross, D. E., and Percival, C. J.: Seasonality of Formic Acid

(HCOOH) in London during the ClearfLo Campaign, Journal of Geophysical Research: Atmospheres, 122, 10.1002/2017jd027064, 2017.
Barnes, I., Solignac, G., Mellouki, A., and Becker, K. H.: Aspects of the atmospheric chemistry of amides, ChemPhyChem, 11, 3844-3857, 10.1002/cphc.201000374, 2010.
Bates, K. H., Jacob, D. J., Cope, J. D., Chen, X., Millet, D. B., and Nguyen, T. B.: Emerging investigator series: aqueous oxidation of isoprene-derived organic aerosol species as a source of atmospheric formic and acetic acids, Environmental Science: Atmospheres, 10.1039/d3ea00076a, 2023.
Benish, S. E., He, H., Ren, X., Roberts, S. J., Salawitch, R. J., Li, Z., Wang, F., Wang, Y., Zhang, F., Shao, M., Lu, S., and Dickerson, R. R.: Measurement report: Aircraft observations of ozone, nitrogen oxides, and volatile organic compounds over Hebei Province, China, Atmospheric Chemistry and Physics, 20, 14523-14545, 10.5194/acp-20-14523-2020, 2020.
Borduas, N., Murphy, J. G., Wang, C., Silva, G. d., Abbatt, J. P. D. J. E. S., and Letters, T.: Gas Phase Oxidation of Nicotine by OH Radicals: Kinetics, Mechanisms, and Formation of HNCO, 3, 327-331, 2016.
Butkovskaya, N. I., Pouvesle, N., Kukui, A., and Le Bras, G.: Mechanism of the OH-Initiated Oxidation of Glycolaldehyde over the Temperature Range 233−296 K, The Journal of Physical Chemistry A, 110, 13492-13499, 10.1021/jp064993k, 2006a.
Butkovskaya, N. I., Pouvesle, N., Kukui, A., Mu, Y., and Le Bras, G.: Mechanism of the OH-Initiated Oxidation of Hydroxyacetone over the Temperature Range 236−298 K, The Journal of Physical Chemistry A, 110, 6833-6843, 10.1021/jp056345r, 2006b.
Chandra, B. P. and Sinha, V.: Contribution of post-harvest agricultural paddy residue fires in the N.W. Indo-Gangetic Plain to ambient carcinogenic benzenoids, toxic isocyanic acid and carbon monoxide, Environment International, 88, 187-197, 10.1016/j.envint.2015.12.025, 2016.
Chebbi, A. and Carlier, P.: Carboxylic acids in the troposphere, occurrence, sources, and sinks: A review, Atmospheric Environment, 30, 4233-4249, https://doi.org/10.1016/1352-2310(96)00102-1, 1996.
Cope, J. D., Abellar, K. A., Bates, K. H., Fu, X., and Nguyen, T. B.: Aqueous Photochemistry of 2-Methyltetrol and Erythritol as Sources of Formic Acid and Acetic Acid in the Atmosphere, ACS Earth and Space Chemistry, 5, 1265-1277, 10.1021/acsearthspacechem.1c00107, 2021.
De Gouw, J. A., Gilman, J. B., Kim, S. W., Alvarez, S. L., Dusanter, S., Graus, M., Griffith, S. M., Isaacman‐VanWertz, G., Kuster, W. C., Lefer, B. L., Lerner, B. M., McDonald, B. C., Rappenglück, B., Roberts, J. M., Stevens, P. S., Stutz, J., Thalman, R., Veres, P. R., Volkamer, R., Warneke, C., Washenfelder, R. A., and Young, C. J.: Chemistry of Volatile Organic Compounds in the Los Angeles Basin: Formation of Oxygenated Compounds and Determination of Emission Ratios, Journal of Geophysical Research: Atmospheres, 123, 2298-2319, 10.1002/2017jd027976, 2018.
Deming, B. L., Pagonis, D., Liu, X., Day, D. A., Talukdar, R., Krechmer, J. E., de Gouw,

J. A., Jimenez, J. L., and Ziemann, P. J.: Measurements of delays of gas-phase compounds in a wide variety of tubing materials due to gas–wall interactions, Atmospheric Measurement Techniques, 12, 3453-3461, 10.5194/amt-12-3453-2019, 2019.

Enders, G., Dlugi, R., Steinbrecher, R., Clement, B., Daiber, R., Eijk, J. v., Gäb, S., Haziza, M., Helas, G., Herrmann, U., Kessel, M., Kesselmeier, J., Kotzias, D., Kourtidis, K., Kurth, H. H., McMillen, R. T., Roider, G., Schürmann, W., Teichmann, U., and Torres, L.: Biosphere/Atmosphere interactions: Integrated research in a European coniferous forest ecosystem, Atmospheric Environment, 26, 171-189, https://doi.org/10.1016/0960-1686(92)90269-Q, 1992.

Fang, X., Shao, M., Stohl, A., Zhang, Q., Zheng, J., Guo, H., Wang, C., Wang, M., Ou, J., Thompson, R. L., and Prinn, R. G.: Top-down estimates of benzene and toluene emissions in the Pearl River Delta and Hong Kong, China, Atmospheric Chemistry and Physics, 16, 3369-3382, 10.5194/acp-16-3369-2016, 2016.

Franco, B., Blumenstock, T., Cho, C., Clarisse, L., Clerbaux, C., Coheur, P. F., De Mazière, M., De Smedt, I., Dorn, H. P., Emmerichs, T., Fuchs, H., Gkatzelis, G., Griffith, D. W. T., Gromov, S., Hannigan, J. W., Hase, F., Hohaus, T., Jones, N., Kerkweg, A., Kiendler-Scharr, A., Lutsch, E., Mahieu, E., Novelli, A., Ortega, I., Paton-Walsh, C., Pommier, M., Pozzer, A., Reimer, D., Rosanka, S., Sander, R., Schneider, M., Strong, K., Tillmann, R., Van Roozendael, M., Vereecken, L., Vigouroux, C., Wahner, A., and Taraborrelli, D.: Ubiquitous atmospheric production of organic acids mediated by cloud droplets, Nature, 593, 233-237, 10.1038/s41586-021-03462-x, 2021.

Fulgham, S. R., Brophy, P., Link, M., Ortega, J., Pollack, I., and Farmer, D. K.: Seasonal Flux Measurements over a Colorado Pine Forest Demonstrate a Persistent Source of Organic Acids, ACS Earth and Space Chemistry, 3, 2017-2032, 10.1021/acsearthspacechem.9b00182, 2019.

Galloway, J. N., Likens, G. E., Keene, W. C., and Miller, J. M.: The composition of precipitation in remote areas of the world, Journal of Geophysical Research: Oceans, 87, 8771-8786, https://doi.org/10.1029/JC087iC11p08771, 1982.

Goode, J. G., Yokelson, R. J., Ward, D. E., Susott, R. A., Babbitt, R. E., Davies, M. A., and Hao, W. M.: Measurements of excess O_3, CO_2, CO, CH_4, C_2H_4, C_2H_2, HCN, NO, NH_3, HCOOH, CH_3COOH, HCHO, and CH_3OH in 1997 Alaskan biomass burning plumes by airborne Fourier transform infrared spectroscopy (AFTIR), Journal of Geophysical Research: Atmospheres, 105, 22147-22166, 10.1029/2000jd900287, 2000.

Grosjean, D., Williams, E. L., II, and Grosjean, E.: Atmospheric chemistry of isoprene and of its carbonyl products, Environmental Science & Technology, 27, 830-840, 10.1021/es00042a004, 1993.

Helmig, D., Johnson, B., Oltmans, S., Neff, W., Eisele, F., and Davis, D.: Elevated ozone in the boundary layer at South Pole, Atmospheric Environment, 42, 2788-2803, 10.1016/j.atmosenv.2006.12.032, 2008a.

Helmig, D., Johnson, B., Warshawsky, M., Morse, T., Neff, W., Eisele, F., and Davis, D.: Nitric oxide in the boundary-layer at South Pole during the Antarctic Tropospheric Chemistry Investigation (ANTCI), Atmospheric Environment, 42, 2817-2830, 10.1016/j.atmosenv.2007.03.061, 2008b.

Hems, R. F., Wang, C., Collins, D. B., Zhou, S., Borduas-Dedekind, N., Siegel, J. A., and Abbatt, J. P. D.: Sources of isocyanic acid (HNCO) indoors: a focus on cigarette smoke, Environmental Science: Processes & Impacts, 21, 1334-1341, 10.1039/c9em00107g, 2019.

Hu, L., Millet, D. B., Kim, S. Y., Wells, K. C., Griffis, T. J., Fischer, E. V., Helmig, D., Hueber, J., and Curtis, A. J.: North American acetone sources determined from tall tower measurements and inverse modeling, Atmospheric Chemistry and Physics, 13, 3379-3392, 10.5194/acp-13-3379-2013, 2013.

Hu, X., Yang, G., Liu, Y., Lu, Y., Wang, Y., Chen, H., Chen, J., and Wang, L.: Atmospheric gaseous organic acids in winter in a rural site of the North China Plain, Journal of Environmental Sciences, 113, 190-203, 10.1016/j.jes.2021.05.035, 2022.

Jacob, D. J.: Chemistry of OH in remote clouds and its role in the production of formic acid and peroxymonosulfate, Journal of Geophysical Research: Atmospheres, 91, 9807-9826, https://doi.org/10.1029/JD091iD09p09807, 1986.

Jaisson, S., Pietrement, C., and Gillery, P.: Carbamylation-derived products: bioactive compounds and potential biomarkers in chronic renal failure and atherosclerosis, Clinical chemistry, 57, 1499-1505, 10.1373/clinchem.2011.163188, 2011.

Jathar, S. H., Heppding, C., Link, M. F., Farmer, D. K., Akherati, A., Kleeman, M. J., de Gouw, J. A., Veres, P. R., and Roberts, J. M.: Investigating diesel engines as an atmospheric source of isocyanic acid in urban areas, Atmospheric Chemistry and Physics, 17, 8959-8970, 10.5194/acp-17-8959-2017, 2017.

Ji, Y., Huey, L. G., Tanner, D. J., Lee, Y. R., Veres, P. R., Neuman, J. A., Wang, Y., and Wang, X.: A vacuum ultraviolet ion source (VUV-IS) for iodide–chemical ionization mass spectrometry: a substitute for radioactive ion sources, Atmospheric Measurement Techniques, 13, 3683-3696, 10.5194/amt-13-3683-2020, 2020.

Karion, A., Sweeney, C., Tans, P., and Newberger, T.: AirCore: An Innovative Atmospheric Sampling System, Journal of Atmospheric and Oceanic Technology, 27, 1839-1853, 10.1175/2010jtecha1448.1, 2010.

Kawamura, K. and Kaplan, I. R.: Organic compounds in the rainwater of Los Angeles, Environmental Science & Technology, 17, 497-501, 10.1021/es00114a011, 1983.

Kawamura, K., Steinberg, S., and Kaplan, I. R.: Homologous series of C_1–C_{10} monocarboxylic acids and C_1–C_6 carbonyls in Los Angeles air and motor vehicle exhausts, Atmospheric Environment, 34, 4175-4191, https://doi.org/10.1016/S1352-2310(00)00212-0, 2000.

Keene, W. C. and Galloway, J. N.: Organic acidity in precipitation of North America, Atmospheric Environment, 18, 2491-2497, https://doi.org/10.1016/0004-6981(84)90020-9, 1984.

Kesselmeier, J., Bode, K., Gerlach, C., and Jork, E. M.: Exchange of atmospheric

formic and acetic acids with trees and crop plants under controlled chamber and purified air conditions, Atmospheric Environment, 32, 1765-1775, https://doi.org/10.1016/S1352-2310(97)00465-2, 1998.

Khare, P., Kumar, N., Kumari, K. M., and Srivastava, S. S.: Atmospheric formic and acetic acids: An overview, Reviews of Geophysics, 37, 227-248, https://doi.org/10.1029/1998RG900005, 1999.

Koeth, R. A., Kalantar-Zadeh, K., Wang, Z., Fu, X., Tang, W. H., and Hazen, S. L.: Protein carbamylation predicts mortality in ESRD, Journal of the American Society of Nephrology, 24, 853-861, 10.1681/ASN.2012030254, 2013.

Krechmer, J. E., Day, D. A., Ziemann, P. J., and Jimenez, J. L.: Direct Measurements of Gas/Particle Partitioning and Mass Accommodation Coefficients in Environmental Chambers, Environmental science & technology, 51, 11867-11875, 10.1021/acs.est.7b02144, 2017.

Le Breton, M., Bacak, A., Muller, J. B. A., Xiao, P., Shallcross, B. M. A., Batt, R., Cooke, M. C., Shallcross, D. E., Bauguitte, S. J. B., and Percival, C. J.: Simultaneous airborne nitric acid and formic acid measurements using a chemical ionization mass spectrometer around the UK: Analysis of primary and secondary production pathways, Atmospheric Environment, 83, 166-175, 10.1016/j.atmosenv.2013.10.008, 2014.

Lei, X., Wang, W., Gao, J., Wang, S., and Wang, W.: Atmospheric Chemistry of Enols: The Formation Mechanisms of Formic and Peroxyformic Acids in Ozonolysis of Vinyl Alcohol, The Journal of Physical Chemistry A, 124, 4271-4279, 10.1021/acs.jpca.0c01480, 2020.

Li, T., Wang, Z., Yuan, B., Ye, C., Lin, Y., Wang, S., Sha, Q. e., Yuan, Z., Zheng, J., and Shao, M.: Emissions of carboxylic acids, hydrogen cyanide (HCN) and isocyanic acid (HNCO) from vehicle exhaust, Atmospheric Environment, 247, 10.1016/j.atmosenv.2021.118218, 2021.

Li, X.-B., Yuan, B., Wang, S., Wang, C., Lan, J., Liu, Z., Song, Y., He, X., Huangfu, Y., Pei, C., Cheng, P., Yang, S., Qi, J., Wu, C., Huang, S., You, Y., Chang, M., Zheng, H., Yang, W., Wang, X., and Shao, M.: Variations and sources of volatile organic compounds (VOCs) in urban region: insights from measurements on a tall tower, Atmospheric Chemistry and Physics, 22, 10567-10587, 10.5194/acp-22-10567-2022, 2022.

Li, X., Zhang, C., Liu, A., Yuan, B., Yang, H., Liu, C., Wang, S., Huangfu, Y., Qi, J., Liu, Z., He, X., Song, X., Chen, Y., Peng, Y., Zhang, X., Zheng, E., Yang, L., Yang, Q., Qin, G., Zhou, J., and Shao, M.: Assessment of Long Tubing in Measuring Atmospheric Trace Gases: Applications on Tall Towers, Environmental Science: Atmospheres, 506-520, 10.1039/d2ea00110a, 2023.

Liggio, J., Moussa, S. G., Wentzell, J., Darlington, A., Liu, P., Leithead, A., Hayden, K., O'Brien, J., Mittermeier, R. L., Staebler, R., Wolde, M., and Li, S.-M.: Understanding the primary emissions and secondary formation of gaseous organic acids in the oil sands region of Alberta, Canada, Atmospheric Chemistry and Physics, 17, 8411-8427,

855 10.5194/acp-17-8411-2017, 2017.
856 Link, M. F., Brophy, P., Fulgham, S. R., Murschell, T., and Farmer, D. K.: Isoprene
857 versus Monoterpenes as Gas-Phase Organic Acid Precursors in the Atmosphere, ACS
858 Earth and Space Chemistry, 5, 1600-1612, 10.1021/acsearthspacechem.1c00093,
859 2021.
860 Link, M. F., Nguyen, T. B., Bates, K., Müller, J.-F., and Farmer, D. K.: Can Isoprene
861 Oxidation Explain High Concentrations of Atmospheric Formic and Acetic Acid over
862 Forests?, ACS Earth and Space Chemistry, 4, 730-740,
863 10.1021/acsearthspacechem.0c00010, 2020.
864 Liu, X., Deming, B., Pagonis, D., Day, D. A., Palm, B. B., Talukdar, R., Roberts, J. M.,
865 Veres, P. R., Krechmer, J. E., Thornton, J. A., de Gouw, J. A., Ziemann, P. J., and
866 Jimenez, J. L.: Effects of gas–wall interactions on measurements of semivolatile
867 compounds and small polar molecules, Atmospheric Measurement Techniques, 12,
868 3137-3149, 10.5194/amt-12-3137-2019, 2019.
869 Lopez-Hilfiker, F. D., Mohr, C., Ehn, M., Rubach, F., Kleist, E., Wildt, J., Mentel, T. F.,
870 Lutz, A., Hallquist, M., Worsnop, D., and Thornton, J. A.: A novel method for online
871 analysis of gas and particle composition: description and evaluation of a Filter Inlet
872 for Gases and AEROsols (FIGAERO), Atmospheric Measurement Techniques, 7,
873 983-1001, 10.5194/amt-7-983-2014, 2014.
874 Mattila, J. M., Brophy, P., Kirkland, J., Hall, S., Ullmann, K., Fischer, E. V., Brown, S.,
875 McDuffie, E., Tevlin, A., and Farmer, D. K.: Tropospheric sources and sinks of gas-
876 phase acids in the Colorado Front Range, Atmospheric Chemistry and Physics, 18,
877 12315-12327, 10.5194/acp-18-12315-2018, 2018.
878 Meng, F., Qin, M., Tang, K., Duan, J., Fang, W., Liang, S., Ye, K., Xie, P., Sun, Y., Xie,
879 C., Ye, C., Fu, P., Liu, J., and Liu, W.: High-resolution vertical distribution and
880 sources of HONO and NO_2 in the nocturnal boundary layer in urban Beijing, China,
881 Atmospheric Chemistry and Physics, 20, 5071-5092, 10.5194/acp-20-5071-2020,
882 2020.
883 Millet, D. B., Baasandorj, M., Farmer, D. K., Thornton, J. A., Baumann, K., Brophy, P.,
884 Chaliyakunnel, S., de Gouw, J. A., Graus, M., Hu, L., Koss, A., Lee, B. H., Lopez-
885 Hilfiker, F. D., Neuman, J. A., Paulot, F., Peischl, J., Pollack, I. B., Ryerson, T. B.,
886 Warneke, C., Williams, B. J., and Xu, J.: A large and ubiquitous source of
887 atmospheric formic acid, Atmospheric Chemistry and Physics, 15, 6283-6304,
888 10.5194/acp-15-6283-2015, 2015.
889 Mungall, E. L., Abbatt, J. P. D., Wentzell, J. J. B., Wentworth, G. R., Murphy, J. G.,
890 Kunkel, D., Gute, E., Tarasick, D. W., Sharma, S., Cox, C. J., Uttal, T., and Liggio,
891 J.: High gas-phase mixing ratios of formic and acetic acid in the High Arctic,
892 Atmospheric Chemistry and Physics, 18, 10237-10254, 10.5194/acp-18-10237-2018,
893 2018.
894 Mydel, P., Wang, Z., Brisslert, M., Hellvard, A., Dahlberg, L. E., Hazen, S. L., and
895 Bokarewa, M. I. J. T. J. o. I.: Carbamylation-Dependent Activation of T Cells: A
896 Novel Mechanism in the Pathogenesis of Autoimmune Arthritis, The Journal of

Immunology, 184, 6882 - 6890, 2010.
Neeb, P., Sauer, F., Horie, O., and Moortgat, G. K.: Formation of hydroxymethyl hydroperoxide and formic acid in alkene ozonolysis in the presence of water vapour, Atmospheric Environment, 31, 1417-1423, https://doi.org/10.1016/S1352-2310(96)00322-6, 1997.
Pagonis, D., Krechmer, J. E., de Gouw, J., Jimenez, J. L., and Ziemann, P. J.: Effects of gas–wall partitioning in Teflon tubing and instrumentation on time-resolved measurements of gas-phase organic compounds, Atmospheric Measurement Techniques, 10, 4687-4696, 10.5194/amt-10-4687-2017, 2017.
Palm, B. B., Liu, X., Jimenez, J. L., and Thornton, J. A.: Performance of a new coaxial ion–molecule reaction region for low-pressure chemical ionization mass spectrometry with reduced instrument wall interactions, Atmospheric Measurement Techniques, 12, 5829-5844, 10.5194/amt-12-5829-2019, 2019.
Paulot, F., Crounse, J. D., Kjaergaard, H. G., Kroll, J. H., Seinfeld, J. H., and Wennberg, P. O.: Isoprene photooxidation: new insights into the production of acids and organic nitrates, Atmospheric Chemistry and Physics, 9, 1479-1501, 10.5194/acp-9-1479-2009, 2009.
Paulot, F., Wunch, D., Crounse, J. D., Toon, G. C., Millet, D. B., DeCarlo, P. F., Vigouroux, C., Deutscher, N. M., Gonzalez Abad, G., Notholt, J., Warneke, T., Hannigan, J. W., Warneke, C., de Gouw, J. A., Dunlea, E. J., De Maziere, M., Griffith, D. W. T., Bernath, P., Jimenez, J. L., and Wennberg, P. O.: Importance of secondary sources in the atmospheric budgets of formic and acetic acids, Atmospheric Chemistry and Physics, 11, 1989-2013, 10.5194/acp-11-1989-2011, 2011.
Roberts, J. M. and Liu, Y.: Solubility and solution-phase chemistry of isocyanic acid, methyl isocyanate, and cyanogen halides, Atmospheric Chemistry and Physics, 19, 4419-4437, 10.5194/acp-19-4419-2019, 2019.
Roberts, J. M., Veres, P. R., Cochran, A. K., Warneke, C., Burling, I. R., Yokelson, R. J., Lerner, B., Gilman, J. B., Kuster, W. C., Fall, R., and de Gouw, J.: Isocyanic acid in the atmosphere and its possible link to smoke-related health effects, Proceedings of the National Academy of Sciences, 108, 8966-8971, 10.1073/pnas.1103352108, 2011.
Roberts, J. M., Veres, P. R., VandenBoer, T. C., Warneke, C., Graus, M., Williams, E. J., Lefer, B., Brock, C. A., Bahreini, R., Öztürk, F., Middlebrook, A. M., Wagner, N. L., Dubé, W. P., and de Gouw, J. A.: New insights into atmospheric sources and sinks of isocyanic acid, HNCO, from recent urban and regional observations, Journal of Geophysical Research: Atmospheres, 119, 1060-1072, 10.1002/2013jd019931, 2014.
Rosanka, S., Vu, G. H. T., Nguyen, H. M. T., Pham, T. V., Javed, U., Taraborrelli, D., and Vereecken, L.: Atmospheric chemical loss processes of isocyanic acid (HNCO): a combined theoretical kinetic and global modelling study, Atmospheric Chemistry and Physics, 20, 6671-6686, 10.5194/acp-20-6671-2020, 2020.
Schnitzhofer, R., Wisthaler, A., and Hansel, A.: Real-time profiling of organic trace gases in the planetary boundary layer by PTR-MS using a tethered balloon,

939 Atmospheric Measurement Techniques, 2, 773-777, 10.5194/amt-2-773-2009, 2009.
940 Schobesberger, S., Lopez‐Hilfiker, F. D., Taipale, D., Millet, D. B., D'Ambro, E. L.,
941 Rantala, P., Mammarella, I., Zhou, P., Wolfe, G. M., Lee, B. H., Boy, M., and
942 Thornton, J. A.: High upward fluxes of formic acid from a boreal forest canopy,
943 Geophysical Research Letters, 43, 9342-9351, 10.1002/2016gl069599, 2016.
944 Skorokhod, A. I., Berezina, E. V., Moiseenko, K. B., Elansky, N. F., and Belikov, I. B.:
945 Benzene and toluene in the surface air of northern Eurasia from TROICA-12
946 campaign along the Trans-Siberian Railway, Atmospheric Chemistry and Physics, 17,
947 5501-5514, 10.5194/acp-17-5501-2017, 2017.
948 Stavrakou, T., Müller, J. F., Peeters, J., Razavi, A., Clarisse, L., Clerbaux, C., Coheur,
949 P. F., Hurtmans, D., De Mazière, M., Vigouroux, C., Deutscher, N. M., Griffith, D.
950 W. T., Jones, N., and Paton-Walsh, C.: Satellite evidence for a large source of formic
951 acid from boreal and tropical forests, Nature Geoscience, 5, 26-30,
952 10.1038/ngeo1354, 2011.
953 Tan, Q., Ge, B., Xu, X., Gan, L., Yang, W., Chen, X., Pan, X., Wang, W., Li, J., and
954 Wang, Z.: Increasing impacts of the relative contributions of regional transport on air
955 pollution in Beijing: Observational evidence, Environmental Pollution, 292, 118407,
956 10.1016/j.envpol.2021.118407, 2022.
957 Verbrugge, F. H., Tang, W. H., and Hazen, S. L.: Protein carbamylation and
958 cardiovascular disease, Kidney International, 88, 474-478, 10.1038/ki.2015.166,
959 2015.
960 Veres, P. R., Roberts, J. M., Cochran, A. K., Gilman, J. B., Kuster, W. C., Holloway, J.
961 S., Graus, M., Flynn, J., Lefer, B., Warneke, C., and de Gouw, J.: Evidence of rapid
962 production of organic acids in an urban air mass, Geophysical Research Letters, 38,
963 L17807, 10.1029/2011gl048420, 2011.
964 Wang, Z., Nicholls, S. J., Rodriguez, E. R., Kummu, O., Horkko, S., Barnard, J.,
965 Reynolds, W. F., Topol, E. J., DiDonato, J. A., and Hazen, S. L.: Protein
966 carbamylation links inflammation, smoking, uremia and atherogenesis, Nature
967 medicine, 13, 1176-1184, 10.1038/nm1637, 2007.
968 Wang, Z., Yuan, B., Ye, C., Roberts, J., Wisthaler, A., Lin, Y., Li, T., Wu, C., Peng, Y.,
969 Wang, C., Wang, S., Yang, S., Wang, B., Qi, J., Wang, C., Song, W., Hu, W., Wang,
970 X., Xu, W., Ma, N., Kuang, Y., Tao, J., Zhang, Z., Su, H., Cheng, Y., Wang, X., and
971 Shao, M.: High Concentrations of Atmospheric Isocyanic Acid (HNCO) Produced
972 from Secondary Sources in China, Environmental Science & Technology, 54, 11818-
973 11826, 10.1021/acs.est.0c02843, 2020.
974 Wentzell, J. J., Liggio, J., Li, S. M., Vlasenko, A., Staebler, R., Lu, G., Poitras, M. J.,
975 Chan, T., and Brook, J. R.: Measurements of gas phase acids in diesel exhaust: a
976 relevant source of HNCO?, Environmental Science & Technology, 47, 7663-7671,
977 10.1021/es401127j, 2013.
978 Woodward-Massey, R., Taha, Y. M., Moussa, S. G., and Osthoff, H. D.: Comparison of
979 negative-ion proton-transfer with iodide ion chemical ionization mass spectrometry
980 for quantification of isocyanic acid in ambient air, Atmospheric Environment, 98,

693-703, 10.1016/j.atmosenv.2014.09.014, 2014.
Wren, S. N., Liggio, J., Han, Y., Hayden, K., Lu, G., Mihele, C. M., Mittermeier, R. L., Stroud, C., Wentzell, J. J. B., and Brook, J. R.: Elucidating real-world vehicle emission factors from mobile measurements over a large metropolitan region: a focus on isocyanic acid, hydrogen cyanide, and black carbon, Atmospheric Chemistry and Physics, 18, 16979-17001, 10.5194/acp-18-16979-2018, 2018.
Wu, C., Wang, C., Wang, S., Wang, W., Yuan, B., Qi, J., Wang, B., Wang, H., Wang, C., Song, W., Wang, X., Hu, W., Lou, S., Ye, C., Peng, Y., Wang, Z., Huangfu, Y., Xie, Y., Zhu, M., Zheng, J., Wang, X., Jiang, B., Zhang, Z., and Shao, M.: Measurement report: Important contributions of oxygenated compounds to emissions and chemistry of volatile organic compounds in urban air, Atmos. Chem. Phys., 20, 14769-14785, https://doi.org/10.5194/acp-20-14769-2020, 2020.
Yan, Y., Wang, S., Zhu, J., Guo, Y., Tang, G., Liu, B., An, X., Wang, Y., and Zhou, B.: Vertically increased NO_3 radical in the nocturnal boundary layer, Science of The Total Environment, 763, 142969, https://doi.org/10.1016/j.scitotenv.2020.142969, 2021.
Yáñez-Serrano, A. M., Nölscher, A. C., Bourtsoukidis, E., Gomes Alves, E., Ganzeveld, L., Bonn, B., Wolff, S., Sa, M., Yamasoe, M., Williams, J., Andreae, M. O., and Kesselmeier, J.: Monoterpene chemical speciation in a tropical rainforest:variation with season, height, and time of dayat the Amazon Tall Tower Observatory (ATTO), Atmospheric Chemistry and Physics, 18, 3403-3418, 10.5194/acp-18-3403-2018, 2018.
Yao, L., Wang, M. Y., Wang, X. K., Liu, Y. J., Chen, H. F., Zheng, J., Nie, W., Ding, A. J., Geng, F. H., Wang, D. F., Chen, J. M., Worsnop, D. R., and Wang, L.: Detection of atmospheric gaseous amines and amides by a high-resolution time-of-flight chemical ionization mass spectrometer with protonated ethanol reagent ions, Atmospheric Chemistry and Physics, 16, 14527-14543, 10.5194/acp-16-14527-2016, 2016.
Yu, S.: Role of organic acids (formic, acetic, pyruvic and oxalic) in the formation of cloud condensation nuclei (CCN): a review, Atmospheric Research, 53, 185-217, https://doi.org/10.1016/S0169-8095(00)00037-5, 2000.
Yuan, B., Koss, A. R., Warneke, C., Coggon, M., Sekimoto, K., and de Gouw, J. A.: Proton-Transfer-Reaction Mass Spectrometry: Applications in Atmospheric Sciences, Chemical reviews, 117, 13187-13229, 10.1021/acs.chemrev.7b00325, 2017.
Yuan, B., Shao, M., de Gouw, J., Parrish, D. D., Lu, S., Wang, M., Zeng, L., Zhang, Q., Song, Y., Zhang, J., and Hu, M.: Volatile organic compounds (VOCs) in urban air: How chemistry affects the interpretation of positive matrix factorization (PMF) analysis, Journal of Geophysical Research: Atmospheres, 117, n/a-n/a, 10.1029/2012jd018236, 2012.
Yuan, B., Veres, P. R., Warneke, C., Roberts, J. M., Gilman, J. B., Koss, A., Edwards, P. M., Graus, M., Kuster, W. C., Li, S. M., Wild, R. J., Brown, S. S., Dubé, W. P., Lerner, B. M., Williams, E. J., Johnson, J. E., Quinn, P. K., Bates, T. S., Lefer, B.,

Hayes, P. L., Jimenez, J. L., Weber, R. J., Zamora, R., Ervens, B., Millet, D. B., Rappenglück, B., and de Gouw, J. A.: Investigation of secondary formation of formic acid: urban environment vs. oil and gas producing region, Atmospheric Chemistry and Physics, 15, 1975-1993, 10.5194/acp-15-1975-2015, 2015.

Zhao, R., Yin, B., Zhang, N., Wang, J., Geng, C., Wang, X., Han, B., Li, K., Li, P., Yu, H., Yang, W., and Bai, Z.: Aircraft-based observation of gaseous pollutants in the lower troposphere over the Beijing-Tianjin-Hebei region, Science of The Total Environment, 773, 144818, 10.1016/j.scitotenv.2020.144818, 2021.

Zhao, R., Lee, A. K. Y., Wentzell, J. J. B., McDonald, A. M., Toom-Sauntry, D., Leaitch, W. R., Modini, R. L., Corrigan, A. L., Russell, L. M., Noone, K. J., Schroder, J. C., Bertram, A. K., Hawkins, L. N., Abbatt, J. P. D., and Liggio, J.: Cloud partitioning of isocyanic acid (HNCO) and evidence of secondary source of HNCO in ambient air, Geophysical Research Letters, 41, 6962-6969, 10.1002/2014gl061112, 2014.

Zhu, B., Han, Y., Wang, C., Huang, X., Xia, S., Niu, Y., Yin, Z., and He, L.: Understanding primary and secondary sources of ambient oxygenated volatile organic compounds in Shenzhen utilizing photochemical age-based parameterization method, Journal of Environmental Sciences (China), 75, 105-114, 10.1016/j.jes.2018.03.008, 2019.

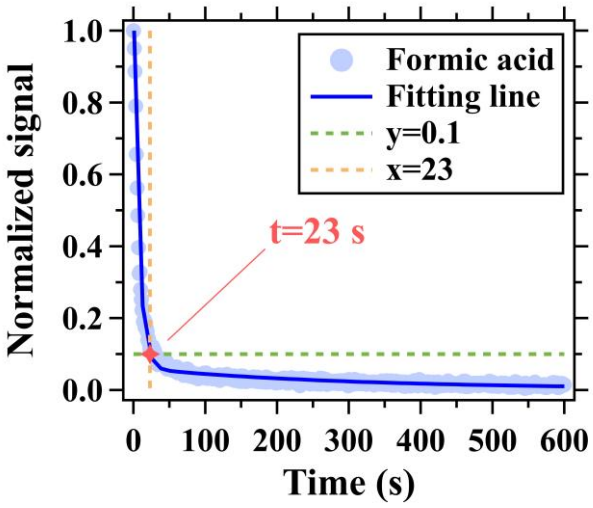

Figure 1. Depassivation curves of formic acid signal measured by I^- ToF-CIMS for the 400 m long tubing at the flow rate of 13 SLPM. Ion signals were normalized to those measured at the start time (0 s) of the step-function change.

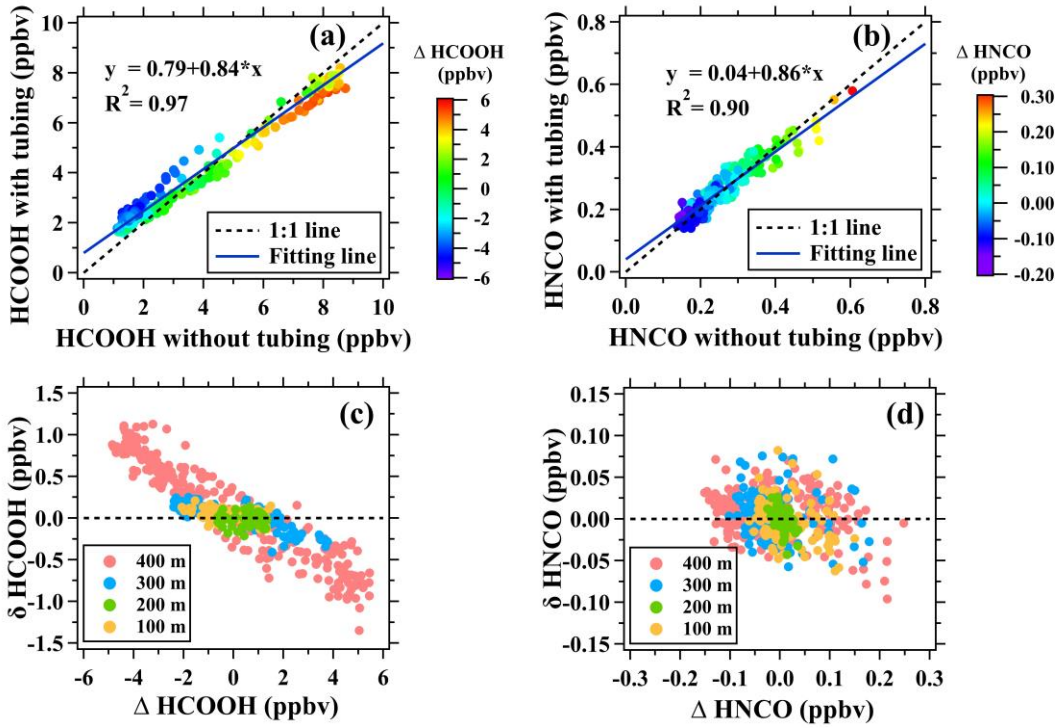

1046

1047 **Figure 2.** Assessment of long tubes in measuring formic and isocyanic acids in ambient
1048 air. (a-b) Scatterplots of mixing ratios of formic and isocyanic acids measured with the
1049 400 m long tube versus those measured without the long tube. (c-d) Scatterplots of
1050 $\Delta[HCOOH]$ versus $\delta[HCOOH]$ and scatterplots of $\Delta[HNCO]$ versus $\delta[HNCO]$ for
1051 the 100, 200, 300, and 400 m tubes.

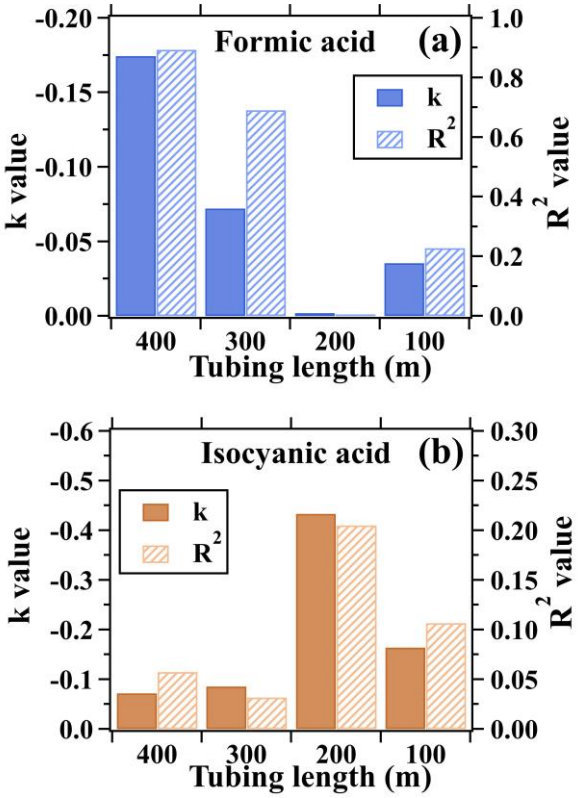

1052

1053 **Figure 3.** Linear fitting parameters (namely k and R^2) for (a) $\Delta[HCOOH]$ versus
1054 $\delta[HCOOH]$ and (b) $\Delta[HNCO]$ versus $\delta[HNCO]$. The scatterplots are shown in
1055 Figure 2. k and R^2 are the slope and determination coefficient of the linear fitting lines,
1056 respectively.

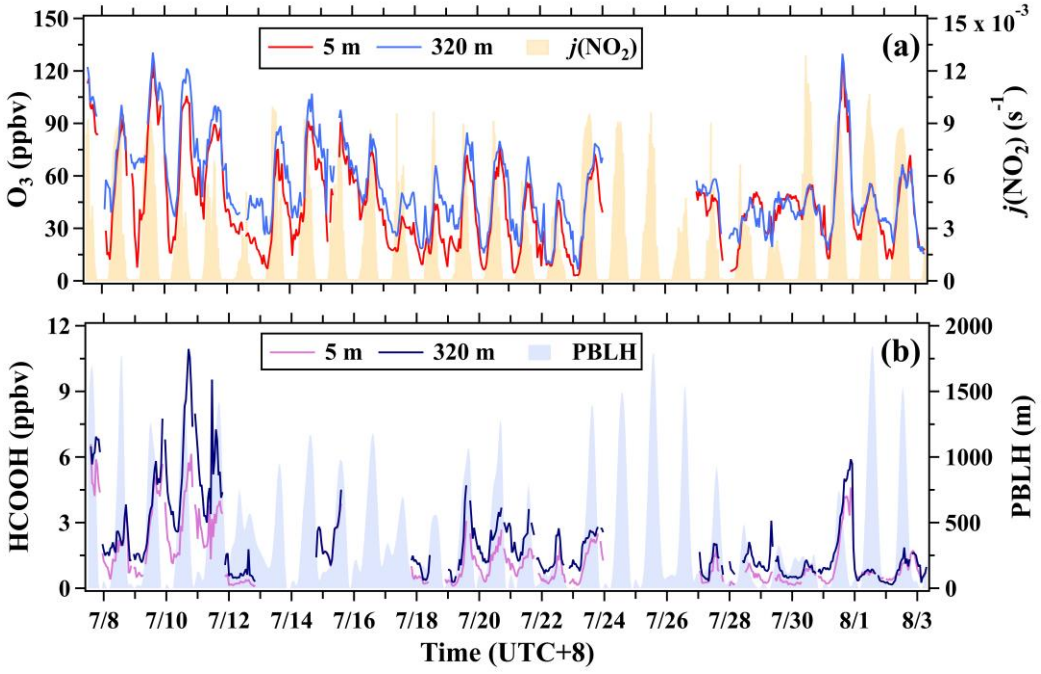

1057

1058 **Figure 4.** Time series of (a) O_3 (5 and 320 m), $j(NO_2)$, (b) formic acid (5 and 320 m),

1059 and planetary boundary layer height (PBLH) during the campaign.

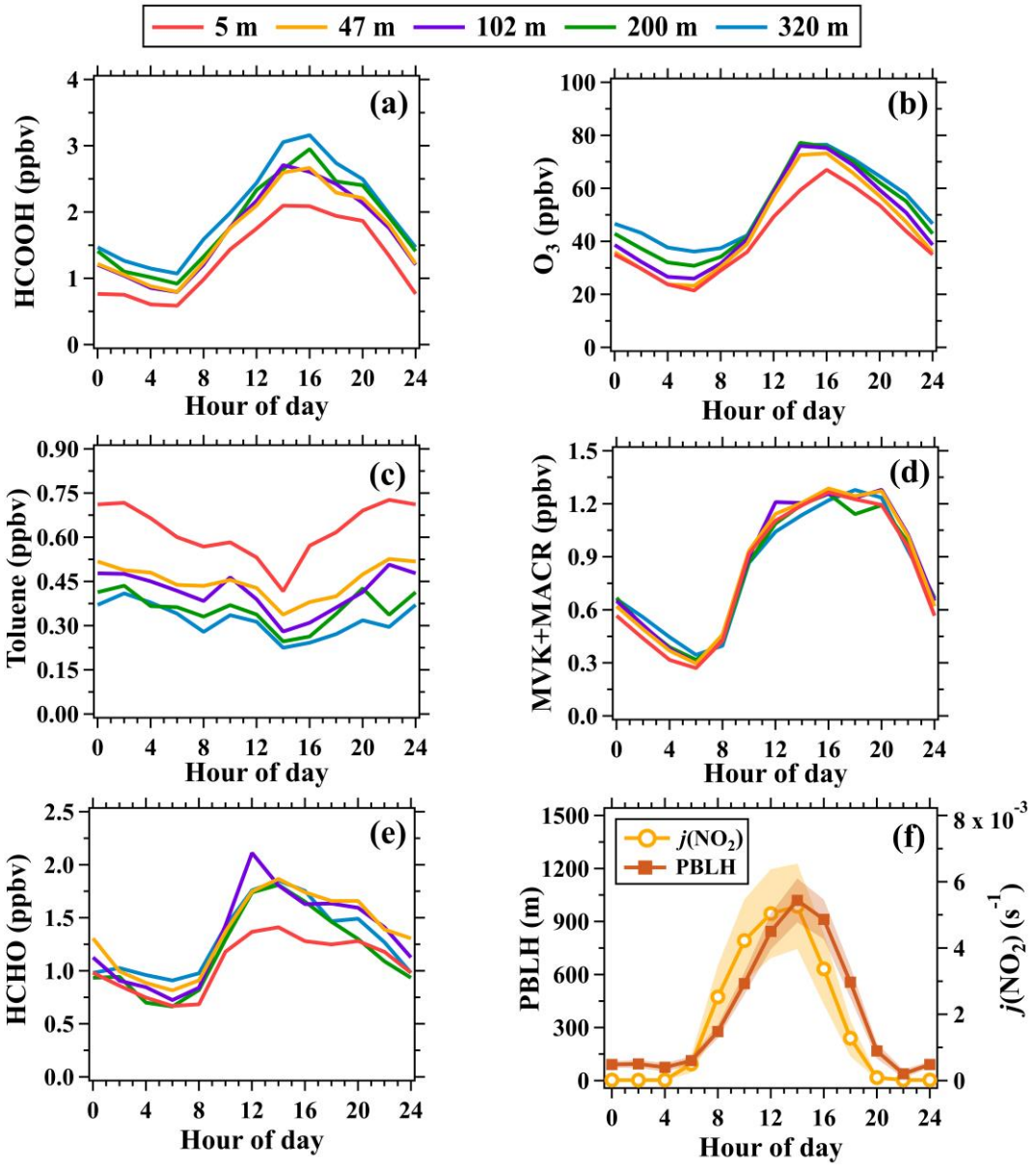

Figure 5. Average diurnal variations in mixing ratios of (a) formic acid, (b) O_3, (c) toluene, (d) MVK+MACR, (e) formaldehyde at the five inlet heights and (f) PBLH and $j(NO_2)$. The shaded areas in panel (f) are half of the standard deviations.

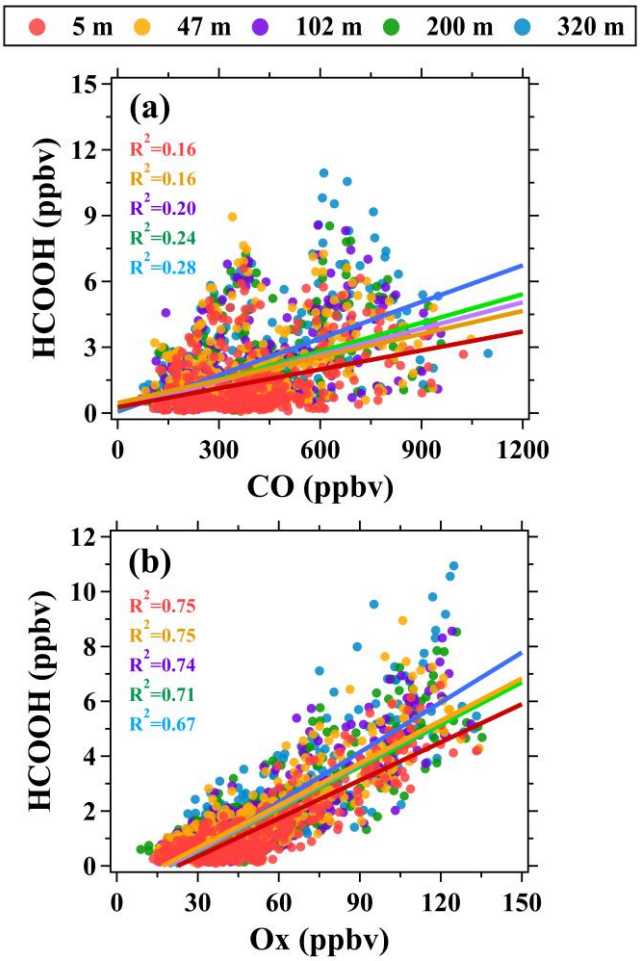

1064

1065 **Figure 6.** Scatter plots of (a) formic acid versus CO and (b) formic acid versus Ox at

1066 different altitudes during the campaign.

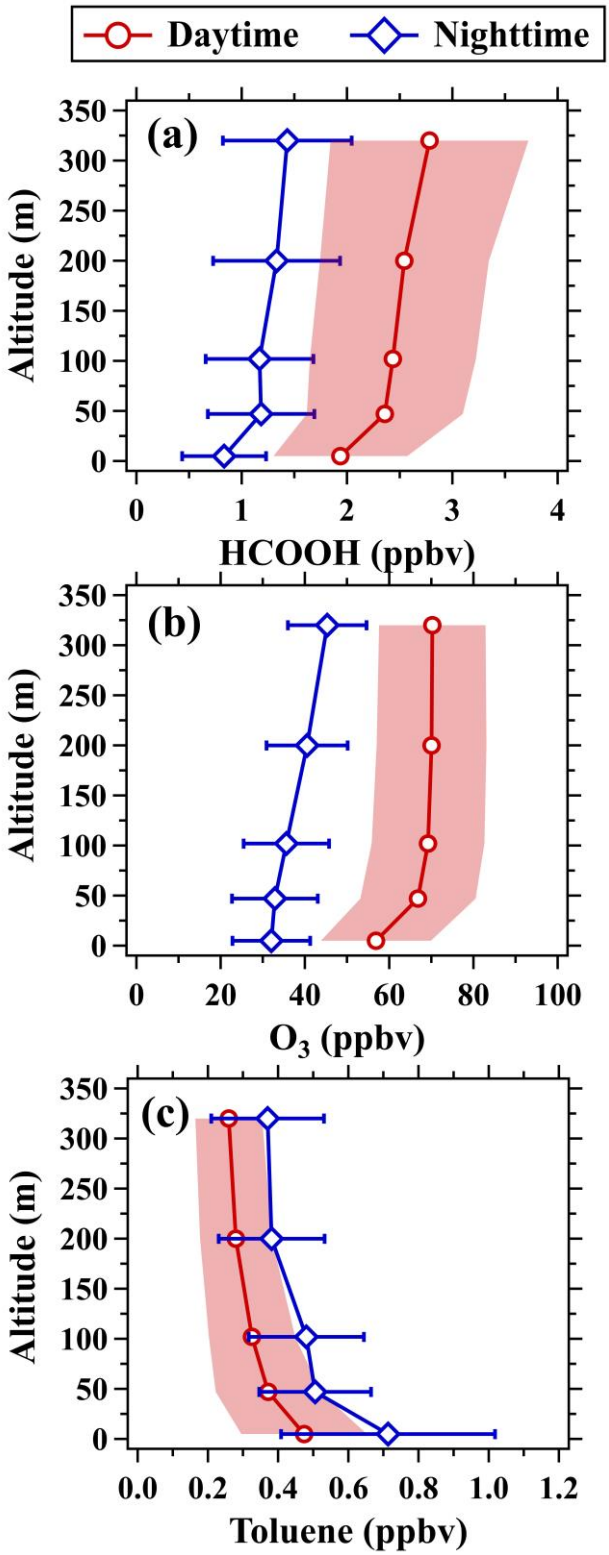

Figure 7. Vertical profiles of (a) formic acid, (b) O_3, and (c) toluene in daytime (11:00-16:00 LT) and nighttime (22:00-5:00 LT). The shaded areas and error bars are half of the standard deviations.

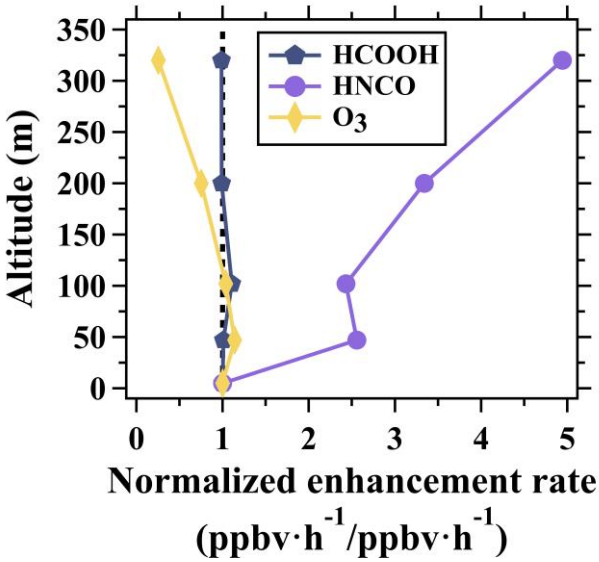

Figure 8. Normalized vertical profiles of the enhancement rate of ozone, formic acid, and isocyanic acid between 6:00-10:00 LT averaged over the whole campaign. Enhancement rate of the species at different altitudes were normalized to those at 5 m. The dotted line indicates the normalized enhancement rate of 1.

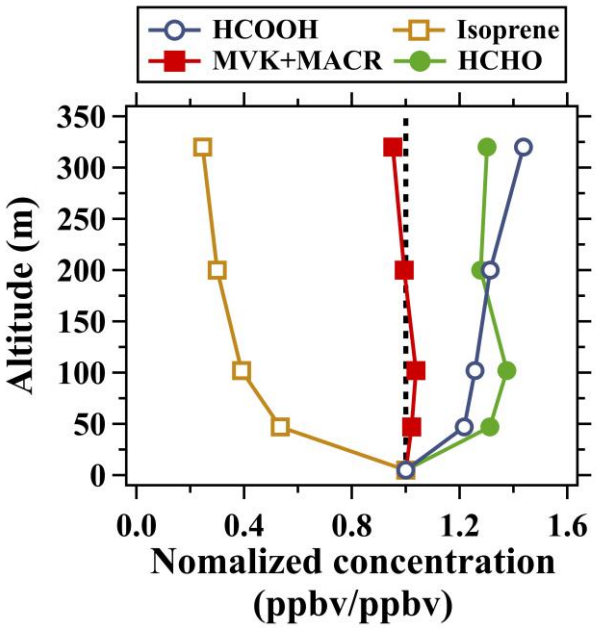

Figure 9. Normalized vertical profiles of formic acid, isoprene, formaldehyde, MVK and MACR in daytime (11:00-16:00 LT) averaged over the whole campaign. Mixing ratios of the species at different altitudes were normalized to those at 5 m. The dotted line indicates the normalized concentration of 1.

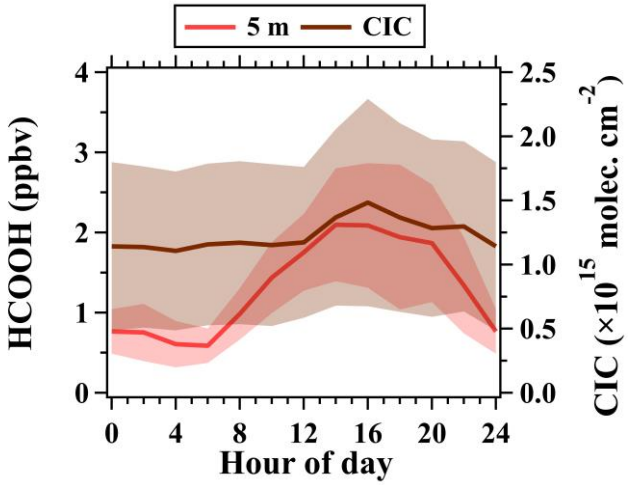

1082

1083 **Figure 10.** Average diurnal variations in mixing ratios (5 m) and CICs of formic acid

1084 during the field campaign; The shaded areas are half of the standard deviations.

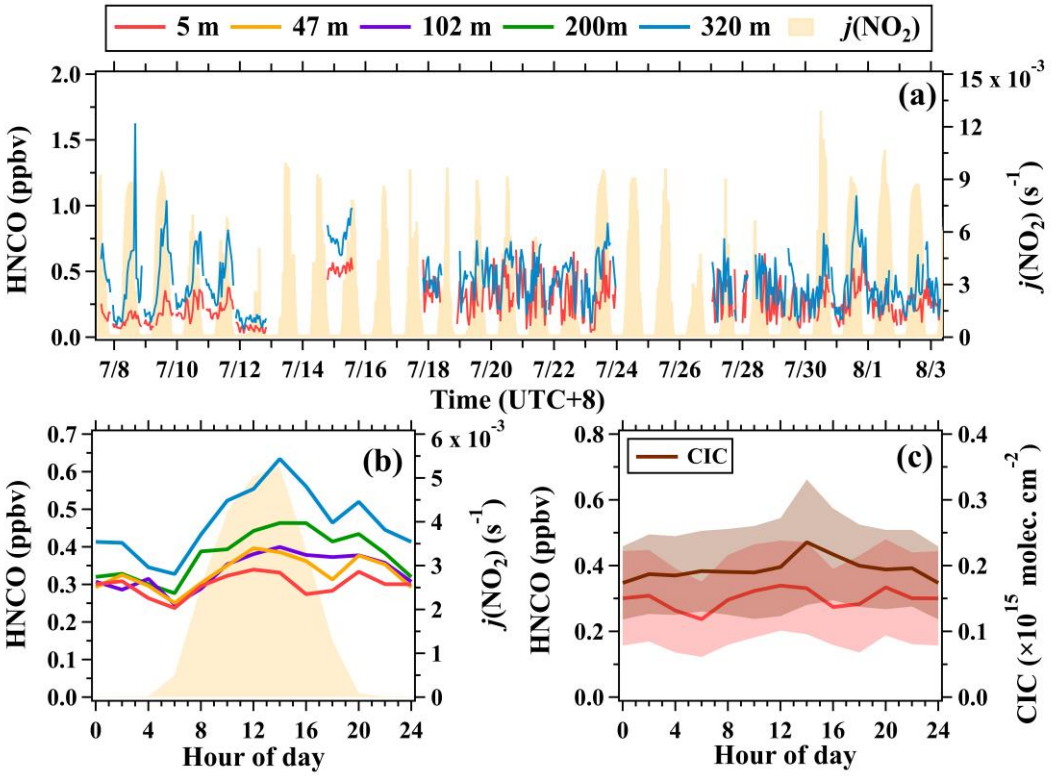

1085

1086 **Figure 11.** (a) Time series of isocyanic acid (5 and 320 m) and *j*(NO_2). (b) Average

1087 diurnal variations in isocyanic acid at 5, 47, 102, 200, and 320 m. (c) Average diurnal

1088 variations in mixing ratios (5 m) and CICs of isocyanic acid during the campaign; The

1089 shaded areas in panel (c) are half of the standard deviations.

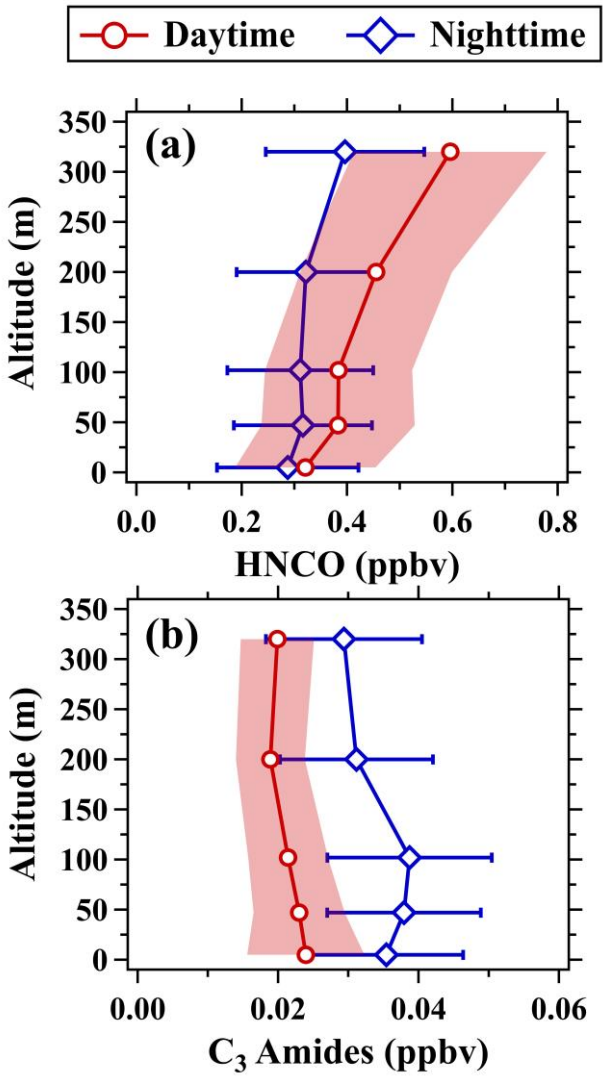

Figure 12. Vertical profiles of (a) isocyanic acid and (b) C_3 amides in daytime (11:00-16:00 LT) and nighttime (22:00-5:00 LT). The shaded areas and error bars are half of the standard deviations.

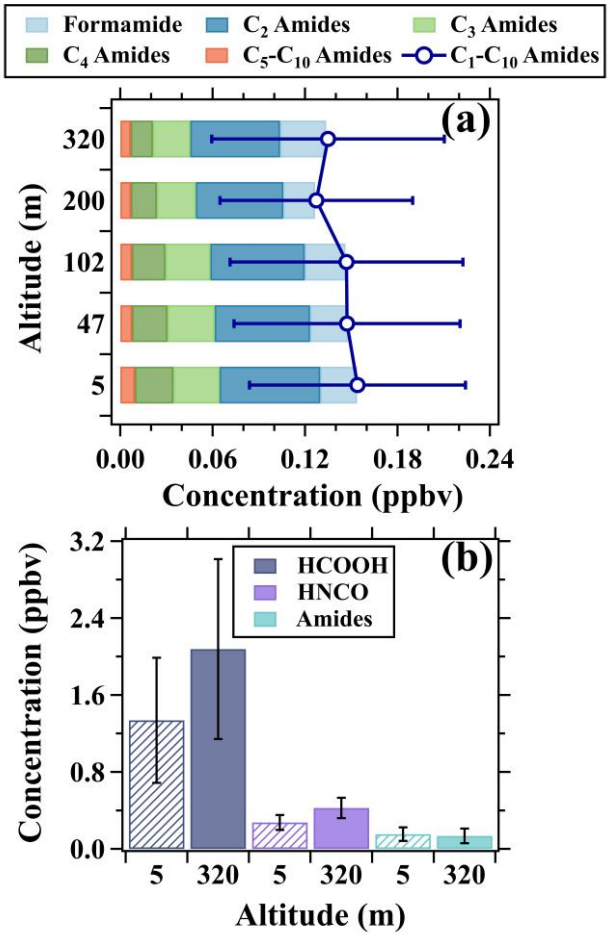

1095

1096 **Figure 13.** (a) Vertical variations in composition and concentrations of amides. (b)
1097 Concentration comparison of formic acid, isocyanic acid, and amides between 5 and
1098 320 m. The data in both (a) and (b) was the average results of the whole campaign. The
1099 patterns of the bars are used to distinguish the average concentration of the species at
1100 the two heights.